INTERNATIONAL ATOMIC ENERGY AGENCY
UNITED NATIONS EDUCATIONAL, SCIENTIFIC AND CULTURAL ORGANIZATION
INTERNATIONAL CENTRE FOR THEORETICAL PHYSICS
I.C.T.P., P.O. BOX 586, 34100 TRIESTE, ITALY, CABLE: CENTRATOM TRIESTE

H4.SMR/942-19

Third Workshop on
3D Modelling of Seismic Waves Generation
Propagation and their Inversion

4 - 15 November 1996

New Constraints on Deep Earth Structure from Generalized Spectral Fitting: Application to Free Oscillations below 3 mHz

J.S. Resovsky, M. H. Ritzwoller

University of Colorado
Dept. of Physics
Boulder, Co
U.S.A.

NEW CONSTRAINTS ON DEEP EARTH STRUCTURE FROM GENERALIZED SPECTRAL FITTING: APPLICATION TO FREE OSCILLATIONS BELOW 3 mHz

Joseph S. Resovsky

and

Michael H. Ritzwoller

University of Colorado

Department of Physics

Campus Box 390

Boulder, CO 80309-0390

to be submitted to

Journal of Geophysical Research

November 1, 1996

New Constraints on Deep Earth Structure from Generalized Spectral Fitting: Application to Free Oscillations below 3 mHz

Abstract

We present the results of generalized spectral fitting (GSF) regressions which estimate normal mode interaction coefficients for the observable spheriodal and toroidal free oscillation multiplets below 3 mHz. This is a set of more than 3000 coefficients for 90 multiplets and 15 coupled pairs, including several deep mantle overtones previously obscured by fundamentals. The coefficients constrain mantle structures of both even and odd spherical harmonic degrees, through degree 12. These new and refined constraints complement existing body and surface wave data sets.

We describe the development of GSF, an adaptation of the established spectral fitting technique which incorporates both Coriolis and structural coupling between multiplets. Estimates of coupling coefficients yield new normal mode constraints for both even and odd-degree structures. GSF improves the accuracy of estimates for nearly degenerate overtone multiplets and for pairs of spheroidal and toroidal fundamentals coupled by the Coriolis force. These enhancements permit the extension of analyses to new multiplets and stuctural degrees not previously estimated.

Several guidelines for the application of GSF are established. The most important of these is the use of an edited, high signal-to-noise data set of more than 4500 records from 37 high-moment events. We demonstrate that the use of geographically diverse data can produce order-of magnitude improvements in matrix stability and coefficient standard deviation.

Coefficient estimates are assessed both quantitatively and qualitatively. Both internal and external consistency of the coefficients are inspected. The improved fits to data spectra are tabulated, using measures of misfits to high signal-to-noise records. Uncertainties are assigned through the application of a Monte-Carlo method which simulates both additive (random) noise and multiplicative (signal generated) noise. The latter represents the impacts of unspecified structures and other theoretical errors.

short title: Generalized Spectral Fitting below 3 mHz
key words: interaction coefficients, multiplet coupling

1 Introduction

The dramatic increase in the quantity, quality, and distribution of broadband seismographic stations, and the occurrence of several very strong earthquakes in the 1990's, have provided thousands of new high signal-to-noise broadband seismograms. These data provide the opportunity for much more detailed analyses of the Earth's free-oscillation spectrum than have been attempted to date. Furthermore, comparisons of recent three-dimensional global models reveal significant ambiguities which emphasize the need for additional normal mode constraints on aspherical structure. Such constraints can be used to assess the models and address persistent questions about correlations and scalings between variations in v_s, v_p, ρ, and topography on internal boundaries [e.g., Ritzwoller and Lavely, 1995]. With these motivations, we have made our goal the establishment of a new, higher quality, and greatly expanded database of normal mode interaction coefficients, the observations of normal mode spectra that serve to constrain three-dimensional Earth structure.

This paper presents the first major steps in that program:

- The development of Generalized Spectral Fitting (GSF), an enhancement of the established Spectral Fitting (SF) technique [Ritzwoller, *et al.*, 1986, 1988; Giardini *et al.*, 1987, 1988; Li *et al.*, 1991; Widmer, *et al.*, 1992a,b; Tromp and Zanzerkia, 1995; He and Tromp, 1996], which incorporates inter-multiplet coupling through aspherical structure and the Coriolis force and a Monte-Carlo error analysis;
- The assembly of an expanded data set of $\sim$ 4500 edited broadband seismograms from 37 strong earthquakes;
- The application of GSF to these data to obtain estimates of more than 3000 new normal mode interaction coefficients from 90 different multiplets with frequencies below 3mHz (Figure 1).

Most of these multiplets sample heretofore poorly constrained structures in the transition zone and lower mantle. Thus, the new coefficient estimates provide an important complement

to existing body and surface wave data. Furthermore, they establish the utility of GSF, which will be employed in future analyses of the normal mode spectrum above 3mHz.

Individual free oscillations, or normal mode singlets, are clustered into spectral multiplets of modes with similar wavelengths and nearly degenerate frequencies. It is these usually unresolved multiplet peaks that characterize typical normal mode spectra, such as that shown in Figure 2a. The first investigations of long period normal modes measured the center frequencies and attenuations of fundamental mode multiplet peaks. Treated as degenerate complex frequencies, these were used in constructing spherically symmetric Earth models such as 1066A (Gilbert and Dziewonski, 1975), PREM (Dziewonski and Anderson, 1981), and the Q models of Widmer *et al.*, 1991. The differences between observed multiplet center frequencies and values predicted by spherical models could then be interpreted as the signature of aspherical structure with several asymptotic approximations [e.g., Jordan, 1978; Dahlen, 1979] and were used to constrain three-dimensional mantle models [e.g. Silver and Jordan, 1981; Masters *et al.*, 1982; Davis, 1985, 1987; Masters and Ritzwoller, 1987]. An approximate description of the Coriolis coupling between fundamental spheroidal (Raleigh-type) and toroidal (Love-type) multiplets was used to correct and re-interpret the center frequency measurements [Masters *et al.*, 1983; Smith and Masters, 1989a,b], but further refinements require a more complete and accurate description of the interaction of normal mode singlets and multiplets.

Broadband digital seismic data became readily available in the late 1970's and early 1980's with the deployment of the GDSN and IDA networks. To take advantage of these data, the techniques of singlet stripping [Ritzwoller *et al.*, 1986; Widmer, *et al.*, 1992a] and Spectral Fitting (SF) [Giardini *et al.*, 1987, 1988; Ritzwoller *et al.*, 1986, 1988; Li *et al.*, 1991] were developed. These were used to observe the spreading, or splitting, of singlet frequencies that was expected to be the dominant effect of aspherical Earth structure on isolated fundamental and overtone multiplets. The observations were reported as interaction coefficients (also called splitting function coefficients or structure coefficients), which are nonlinearly related to the observed multiplet spectra, but are linear functionals of Earth structure. These coefficients became new constraints on Earth structure at spherical harmonic degrees $s = 2$ and $s = 4$, and were employed in the construction of three-dimensional mantle models such as SH.10c.17 [Masters *et al.*, 1992] and S16B30 [Masters *et al.*, 1996]. The utility of interaction coefficient estimates from SF was limited by the relatively small

number of multiplets analyzed, by the isolated multiplet approximation which de-emphasized the importance of amplitude perturbations in normal mode spectra and confined the modal constraints to even-degree structures, and by the aliasing of the signals of higher structural degrees into the degree 2 and 4 coefficient estimates.

More accurate and detailed analyses of the normal mode spectrum require data sets of a size and quality that have only recently become available. For this reason, most recent aspherical Earth models, including S12_WM13 [Su, *et al.*,, 1994], MK12_WM13 [Su and Dziewonski, 1996], and SAW12D [Li and Romanowicz, 1996], have been constrained to fit only body and surface wave data, which are complements to normal mode observations. Even models that incorporate normal mode constraints, such as S16B30, use interaction coefficients that are, for the most part, almost a decade old. It is not surprising, therefore, that correlations between various models, exemplified by Figure 3, are poorest at depths best sampled by normal modes. Additionally, as illustrated in Figure 2, seismic spectra below 3 mHz are not as well fit by model predictions as might be expected. There is a clear need for an improved set of normal mode interaction coefficients for this spectral regime, which can be used:

- to assess existing models of v_s and v_p structures in the mantle (*e.g.*, Ritzwoller and Lavely, 1995);
- in new inversions for 3-D models, which may be constrained to be geodynamically consistent [*e.g.*, Ritzwoller and Wahr, 1994];
- to explore the possibility of using normal mode constraints to obtain independent models of aspherical density structures [*e.g.*, Ritzwoller and Wahr, 1995].

The generalization of Spectral Fitting and the newly estimated interaction coefficients presented in this study, therefore, represent a necessary step forward in the evolution of the estimation and application of normal mode constraints on the structure of the deep Earth. The GSF technique enables us to extract much more information from normal mode spectra, in the form of new interation coefficient estimates, than had been possible with traditional SF methods. GSF also allows us to refine earlier interaction coefficient estimates which had been biased by structural signals unspecified in earlier regressions.

The most significant innovation of GSF is the incorporation of coupling between the

modes of different multiplets. This inter-multiplet or cross-coupling, as opposed to the self-coupling interactions of modes within an isolated multiplet, permits much more accurate interpretations of spectral amplitudes. It is also the only means by which interaction coefficients sensitive to odd-degree Earth structures may be estimated. These considerations were discussed in Resovsky and Ritzwoller [1995a], which introduced the inclusion of multiplet cross-coupling in Spectral Fitting techniques, and presented the first estimates of normal mode constraints on odd-degree structures.

The incorporation of cross-coupling also leads to improved estimates of interaction coefficients for fundamental modes coupled by the Coriolis force [Resovsky and Ritzwoller, 1995b]. These estimates, in turn, can be used to construct the synthetic spectra needed to reduce the strong spectral signals of fundamental modes that interfere with the analysis of the more weakly excited overtones. GSF coefficient estimates are better at this than model predictions. Additionally, the reduction of the bias in self-coupled interaction coefficient estimates by multiplet interference and by previously unestimated cross-coupling allows us to report estimates for coefficients through spherical harmonic degree 12. The rationale for such an extension of the estimates beyond degree 4 was discussed by Ritzwoller and Resovsky [1995].

In addition to presenting the normal mode interaction coefficients that result from GSF, this paper provides qualitative and quantitative assessments of the estimated coefficients (Section 6). We employ standard statistical tools as well as inspection of the consistency of the estimated coefficients and comparisons of the estimates to model predictions. In the error analysis of Section 7, we demonstrate the augmentation of standard statistical measures of uncertainty with a Monte Carlo method for the estimation of biases. This method incorporates readily observable properties of the data and the GSF residuals in an attempt to circumvent the problem of incomplete knowledge of the error sources. In particular, we argue that the coefficient bias caused by unmodeled structures and methodological errors can be synthesized using statistical properties of misfits to the high signal-to-noise spectra from recent large events. This procedure is combined with an appropriate additive random noise model to yield suites of synthetic data used to characterize uncertainties in the estimated coefficients.

Section 2 defines the terminology and methodology of GSF regressions for normal mode interaction coefficient estimates. Section 3 describes the assembly and processing of the

broadband data set used for our free oscillation studies. Section 4 discusses the technical challenges addressed in obtaining the new interaction coefficients. Particular attention is given to the nature of covariances in the regressions, and the necessity of employing data with a diverse distribution of seismic sources. Regression inputs, coefficient estimates, and data misfits are discussed in Section 5. Section 6 provides assessments of the estimated coefficients, including examinations of the internal consistency of the results and comparisons with model predictions. Section 7 provides the error analysis for the GSF estimates, including a description of the Monte Carlo technique employed in assigning uncertainties.

2 Methodology

2.1 The normal mode interaction matrix

Starting from a spherically symmetric, isotropic, anelastic Earth model, designated by $\mathbf{m}_0(r) = [\kappa_0(r), \mu_0(r), \rho_0(r)]$, an aspherical isotropic elastic Earth model is described by $\mathbf{m}(\mathbf{r}) = \mathbf{m}_0(r) + \delta\mathbf{m}(r, \theta, \phi)$, and by a set of two-dimensional perturbations, $h_d(\theta, \phi)$, to the radii of discontinuities (r_d) in the structural parameters. The perturbations to the spherical model may be represented as sums of spherical harmonic components:

$$\delta\mathbf{m}(\mathbf{r}) = \sum_{s,t} [\delta\kappa_s^t(r), \delta\mu_s^t(r), \delta\rho_s^t(r)] Y_s^t(\theta, \phi) \quad \text{and} \quad h_d(\theta, \phi) = \sum_{s,t} h_{sd}^t Y_s^t(\theta, \phi)\,, \tag{1}$$

where s (≥ 0)and t ($|t| \leq s$) index, respectively, the angular and azimuthal orders of the complex spherical harmonics, $Y_s^t(\theta, \phi)$, which are normalized according to the convention of Edmonds [1960].

Free oscillation multiplets of the spherical model are identified by the radial and angular orders, $(n, l) \equiv k$, of their eigenfunctions, and comprise $2l + 1$ degenerate singlet modes, referred to by azimuthal index m. Assuming that aspherical perturbations to Earth structure are relatively small, the singlets of a rotating aspherical Earth model have frequencies near to the degenerate frequencies of the corresponding spherical Earth multiplets, and their eigenfunctions are linear combinations of those of the spherical earth modes. The expansion coefficients of these linear combinations are the components of the eigenvectors of an interaction matrix, $\mathbf{Z}$, with elements:

$$Z_{nn'll'}^{mm'} = C_{nn'l}^{m} \delta_{ll'} \delta_{mm'} + \sum_{s,t} \Gamma_{ll's}\, c_{s(nn'll')}^{t}\,. \tag{2}$$

Modal frequencies are determined by the eigenvalues of this matrix.

The C term of equation (2) includes the effects of multiplet spacing and of the Earth's rotation and ellipticity, while the Γ factors are analytic functions that result from the geometry of the spherical harmonic basis functions. These factors multiply interaction coefficients of the form,

$$c^t_{s(kk')} = \int_0^{r_E} \delta \mathbf{m}^t_s(r) \cdot \mathbf{M}_{s(kk')}(r)\ r^2 dr\ + \sum_d h^t_{sd} B_{sd(kk')} r^2_d\ , \tag{3}$$

with structural kernels, $\mathbf{M}_{s(kk')}(r) = [K_s(r), M_s(r), R_s(r)]_{(kk')}$, and boundary factors, $B_{sd(kk')} = [K_{sd}, M_{sd}, R_{sd}]_{(kk')}$, that are known functions of the radial eigenfunctions of the modes. The interaction coefficients are linear functionals of aspherical structure which summarize the impact of structural perturbations on the modes. (Since they represent the "interaction" between two coupled modes we refer to them by the name "interaction coefficient" rather than the more common "structure coefficient" or "splitting function coefficient".) This theory is presented in full in Woodhouse and Dahlen [1978] and Woodhouse [1980].

Each element of $\mathbf{Z}$ describes the interaction of a pair of normal modes through aspherical structure. The spectral impacts of these interactions, or couplings, vary inversely with the frequency difference between the singlets. Normal mode spectra, therefore, are often approximated using truncated interaction matrices, in which it is assumed that only $k = k'$ terms in equations (2) and (3) are non-zero. This is the multiplet self-coupling approximation employed in most normal mode studies. More accurate synthetic formalisms employ interaction matrices in which both self-coupling and multiplet cross-coupling ($k \neq k'$) terms are computed for sets of two or more multiplets [e.g., Park, 1986; Park and Gilbert, 1986; Resovsky and Ritzwoller, 1994]. Matrices are truncated only by assuming that these subsets of simultaneously self- and cross-coupled multiplets are isolated from one another in frequency. Synthetic experiments inform the choice of coupling scheme employed for the analysis of each spectral window.

Geometric selection rules included in the Γ factors of equation (2), determine which aspherical structures can affect each form of modal coupling. For each pair (k, k') of multiplets the structural degrees that can contribute to coupling are confined to $|\ l - l'\ | \leq s \leq (l + l')$. Additionally, for multiplet self-coupling, $\Gamma = 0$ when s is odd, and the interaction coefficients depend upon only even-degree structures up to $s = 2l$. The use of the self-coupling approximation has confined most normal mode studies to date to estimate constraints only

on even degrees of aspherical Earth structure.

For cross-coupling of spheroidal modes, $k \neq k'$ and $\Gamma = 0$ for $(l + l' + s)$ odd. In the case of the cross-coupling of spheroidal-toroidal multiplet pairs, $\Gamma = 0$ for $(l + l' + s)$ even. For example, nonzero interaction coefficients of the overtone pair ${}_1S_5 - {}_2S_4$ exist only for $s = 1, 3, 5, 7, 9$, and those for ${}_4S_4 - {}_1T_8$ are at $s = 5, 7, 9$. Interaction coefficient estimates for these types of cross-coupling, which have been made only after the introduction of GSF [Resovsky and Ritzwoller, 1995a], constitute the only normal mode constraints on odd-degree structures. Cross-coupled interaction coefficients can also constrain even-degree structures. For example, coupling coefficients of the multiplet pair ${}_0S_{11} - {}_2S_7$ are nonzero only for even harmonic degrees $s = 4$ through $s = 18$, and those for ${}_0T_{12} - {}_2S_7$ exist only at even degrees $s = 6$ through $s = 18$. Finally, it should be noted that in the 1.5 to 3.0 mHz range, the cross-coupling of fundamental multiplet pairs of the form ${}_0S_l - {}_0T_{(l+1)}$ is dominantly produced by the Coriolis force.

Using the interaction matrix to describe the modes of an aspherical Earth model, a synthetic seismogram for a receiver at position $\mathbf{r}_R$ is given by equation:

$$s(\mathbf{r}_R, t) = \mathcal{R} \cdot e^{i\mathbf{Z}t} \cdot \mathcal{S} \,, \tag{4}$$

where, as in Woodhouse and Girnius [1982], $\mathcal{R}$ is a receiver vector combining instrument response information with modal displacement eigenfunctions at the receiver, while $\mathcal{S}$ is a product of the moment and strain tensors at the source location.

2.2 Regressions for interaction coefficients

In SF, as described by Ritzwoller *et al.* [1986,1988], Giardini *et al.* [1987,1988], and Li *et al.* [1991], and in GSF, interaction coefficients are estimated by linearizing their effect on the data. The spectral residual of record j, produced by estimates of the coefficients after $n-1$ iterations, is $\Delta s_j^{(n)}(\omega_i) = s_j^{\text{data}}(\omega_i) - s_j^{(n-1)}(\omega_i)$, for each discrete frequency (index i) in the band around the targeted group of multiplets. For SF or GSF, gaps and edits of the data timeseries are included in the synthetic timeseries before data and synthetics are transformed and compared in the frequency domain.

The interaction coefficients of the next iteration are given by $c_{s(kk')}^{t(n)} = c_{s(kk')}^{t(n-1)} + \delta c_{s(kk')}^{t(n)}$,

where the perturbations are estimated using the first-order approximation:

$$\Delta s_j^{(n)}(\omega_i) = \sum_k \sum_{s,t} \left[\frac{\partial s_j(\omega_i)}{\partial c^t_{s(k)}} \right]^{(n)} \delta c^{t\,(n)}_{s(k)} + \sum_k \sum_{k' \neq k} \sum_{s,t} \left[\frac{\partial s_j(\omega_i)}{\partial c^t_{s(kk')}} \right]^{(n)} \delta c^{t\,(n)}_{s(kk')} . \tag{5}$$

The right side of equation (5) is separated into sums over perturbations to the self-coupled and cross-coupled interaction coefficients of the targeted multiplets. The interaction coefficients for self-coupling are referred to with a single multipet index, k. For GSF, the partial derivatives of equation (5) are approximated with finite differences. This first-order approximation which incorporates cross-coupling contrasts with the second-order approximation of He and Tromp [1996], which ignores the first-order effects of cross-coupling.

Equation (5) is equivalent to a matrix equation of the form $\Delta \mathbf{s}^{(n)} = \mathbf{A}^{(n)} \cdot \delta \mathbf{c}^{(n)}$. The residual vector, $\Delta \mathbf{s}^{(n)}$, has an element for each frequency of each spectrum, and the perturbation vector, $\delta \mathbf{c}^{(n)}$, has an element for each self-coupled or cross-coupled interaction coefficient. $\mathbf{A}^{(n)}$ is the matrix of partial derivatives. In practice, the regressions employ a weight, w_j, for each spectrum, as described in Section 4.5. These row weights become the nonzero elements of a diagonal matrix, $\mathbf{W}$, that modifies the matrix equation. With iteration indices now dropped, equation (5) becomes:

$$\mathbf{W} \cdot \Delta \mathbf{s} = \mathbf{W} \cdot \mathbf{A} \cdot \delta \mathbf{c} \, . \tag{6}$$

$\mathbf{W} \cdot \mathbf{A}$ is referred to as the regression matrix. For each iteration of GSF, the singular-value decomposition (SVD) of the regression matrix is used to find the perturbation estimates according to:

$$\delta \mathbf{c} = \mathbf{V} \cdot \mathbf{\Lambda}^{-1} \cdot \mathbf{U}^{\mathrm{T}} \cdot \mathbf{W} \cdot \Delta \mathbf{s} \, . \tag{7}$$

$\mathbf{W} \cdot \mathbf{A}$ is decomposed by the rectangular matrix $\mathbf{U}$, the square matrix $\mathbf{V}$, and the diagonal matrix of singular values, $\mathbf{\Lambda} = \delta_{pq} \lambda_p$. The stability of the algorithm is enhanced by normalizing the square of the Euclidean norm of each column of $\mathbf{W} \cdot \mathbf{A}$ [Lawson and Hanson, 1974]. Additionally, such regressions are often damped by ranking and tapering the set of singular values [e.g., Gilbert, 1971]. Our applications of GSF to date have required only the truncation of the columns of V corresponding to a few small singular values. With appropriate input data, variable specification, and weighting, these perturbations $\delta \mathbf{c}^{(n)}$ yield a convergent series of iterative improvements to the coefficient estimates which satisfies certain standards of improved data fit, low variance, and low covariance. These considerations are discussed further in Section 4.

Successful GSF regressions provide sets of interaction coefficient estimates for each targeted self-coupled multiplet and cross-coupled multiplet pair. These coefficients may be displayed in map format using generalized splitting functions:

$$F_{kk'}(\theta,\phi) = \sum_{s,t} c^t_{s(kk')} Y^t_s(\theta,\phi)\,. \tag{8}$$

This is a simple generalization of the self-coupling splitting functions defined by Giardini *et al.* [1987]. These functions, which have units of frequency (μHz), are the normal mode analogue of surface wave phase and group velocity maps, and display the structure of the earth under each point, averaged by the depth sensitivity kernels of the multiplets in question. Figure 12 displays a number of estimated splitting functions.

2.3 Capabilities of GSF

In SF, only the first term on the right of equation (5) is employed in constructing the regressions, so that only the self-coupled ($k' = k$) interaction coefficients of equations (2) and (3) are estimated. This approximation yields constraints on only even-degree aspherical structures. When cross-coupling appreciably impacts spectra, the self-coupling approximation results in significantly biased estimates of self-coupled interaction coefficients. This has been demonstrated for both closely spaced overtone multiplets [Ritzwoller *et al.*, 1988; Resovsky and Ritzwoller, 1995a], and Coriolis-coupled fundamentals [Ritzwoller *et al.*, 1988]. Figure 4 shows how neglecting Coriolis coupling in the GSF regression produces biased interaction coefficient estimates for two pairs of coupled spheroidal and toroidal modes. Strong biases occur not only in the degenerate frequency, Q, and zonal interaction coefficients, but extend to all coefficients since GSF fits amplitudes as well as phases.

In contrast, in GSF all forms of multiplet coupling may be included for two or more multiplets, and the interaction coefficients for the self-coupling and cross-coupling of all the specified multiplets may be estimated simultaneously. The cross-coupled coefficients posses unique depth dependencies at both even and odd degrees since the integral kernels for a cross-coupling multiplet pair are hybrids of those for the self-coupling of the individual multiplets in the pair. Figure 12 shows several examples of coupling kernels.

GSF explicitly incorporates the contribution of the Coriolis force in spheroidal-toroidal multiplet coupling. This has permitted us to refine interaction coefficient estimates for the

fundamental mode multiplets between 1.5 and 3 mHz [Resovsky and Ritzwoller, 1995b]. These multiplets are well excited and overlap most overtone multiplets within the 1.5-3 mHz spectral band. Accurate estimates of interaction coefficients for the overtones can be obtained only if most of the signal of the fundamental modes can be removed using accurate synthetics. GSF estimates for the fundamentals fit the data considerably better than do model predictions (Figure 2), and successfully produce synthetics that reduce fundamental mode interference on overtones. These synthetics are used to retrieve the first interaction coefficient estimates for several overtone multiplets, and for extending and refining coefficient estimates for other sets of overtones.

Biases in interaction coefficient estimates due to unmodeled structures tend to be greatest for the highest degrees estimated, as demonstrated in Table 2. GSF significantly reduces biases formerly produced by cross-coupling and by the interference of strong fundamentals in overtone estimates. With adequate data, therefore, it is possible to use GSF to estimate interaction coefficients for degrees above $s = 4$ with biases at or below the level associated with earlier estimates for degrees 2 and 4. Additionally, estimates of the higher degree coefficients further reduce the level of bias present in degree 2 and 4 estimates. The bias likely to remain in GSF estimates is discussed in Section 7. Section 4 addresses issues of matrix stability and covariance associated with the large regressions required for estimates of $s > 4$ interaction coefficients.

Other capabilities of GSF, which will be described and exploited in future submissions, include the simultaneous estimation of interaction coefficients and corrections to source parameters, and the estimation of the interaction coefficients for aspherical anelastic structure.

3 An edited broadband data set

A primary motivation for the development of generalized spectral fitting has been the need to reduce biases that can result from modal coupling and unspecified structures. In particular, biases produced by previously unconstrained structures are lowered by estimating new coefficients corresponding to those structures. For this reason, it is often desirable to perform GSF regressions for 250 to 300 coefficients simultaneously. This represents an order of magnitude increase in the number of variables in each regression, compared to spectral fitting regressions of a decade ago [e.g., Ritzwoller *et al.*, 1988]. The data set employed,

therefore, must be significantly improved in both quantity and quality.

The recent deployment of many new broadband instruments and the occurrence of dozens of strong events in the late 1980's and early 1990's, displayed in Figure 5 and Table 1, have created a sizeable raw data set. However, as demonstrated in Figure 6, many recordings become useful only after careful hand editing which removes clipped data, calibration pulses, glitches, large aftershocks, and extraneous events. Strong tidal signals must also be removed, to prevent their spectral sidelobes from contaminating the targeted frequency band. Another concern is that the fitting of normal mode multiplets is slowed, and not particularly enhanced, by the inclusion of low signal-to-noise recordings. For computational efficiency, therefore, it is advantageous to inspect the available spectra for each multiplet group and select for analysis only those with relatively high signal-to-noise ratios (SNR).

To address these needs, a total of nearly 4500 long-period or broad-band recordings for 37 major events have been assembled, edited, and detided, with between 50 and 300 seismograms associated with each event. These data, summarized by Table 1, come from the IDA, IRIS-GSN, and GEOSCOPE databases. All gaps in the timeseries, both those of the original data and those produced by edits, are recorded for use in GSF regressions. From the spectra of this data set, high SNR subsets of between 50 to 2000 records have been selected for each separate group of multiplets analyzed. Table 3a describes the nature of the data subset used in each GSF regression. Note that at least two, and usually more than a dozen events provide data for each regression. As discussed in Section 4.1, such diversity of sources proves essential in achieving reliable estimates for large variable sets.

4 Guidelines for Proscribing and Performing GSF Regressions

The goal of GSF applied to the free-oscillation spectrum below 3 mHz is to estimate a set of normal mode interaction coefficient that is as extensive, as precise, and as accurate as possible. This goal can be achieved with a combination of careful *a priori* selection of regression inputs and detailed *a posteriori* assessments of the coefficient estimates and other regression outputs. The inputs include certain choices of: the time series window, the subset of data distinguished by source depth and instrument orientation, the data weighting and the regression damping schemes. Because the data are usually insufficient to estimate the full set of interaction coefficients that affect all the modes within each spectral window, and because

unspecified structures can significantly bias coefficient estimates, variable specification is another important decision in setting up each regression. In addition to interaction coefficient estimates, important GSF outputs include residual misfits to the complex data spectra and the characteristics of the regression matrices.

In the absence of significant and complex sources of systematic error, standard statistical estimates of variance and covariance provide reliable information to guide both input selection and output assessment. When an SVD is employed the estimated covariance matrix is:

$$C_{ij}^{\mathbf{est}} = \sum_p \frac{1}{\lambda_p^2} V_{ip} V_{jp} \,, \tag{9}$$

where V_{ij} and λ_i are defined by equations (6) and (7), and the diagonal elements of $\mathbf{C}$ provide estimates of the coefficient variances. Unfortunately, interaction coefficient estimates can be strongly biased by unspecified short-wavelength structures, by anelastic and anisotropic structures, and by errant source solutions and receiver functions. Standard estimates of variance and covariance have repeatedly proven inadequate for explaining the observed inconsistencies in normal mode observations [*e.g.,* Ritzwoller, et al., 1988]. For example, when data from a large number of events are included in the regression matrix, the coefficient standard deviations, shown in Figure 8 and discussed below, are simply too small, as demonstrated by synthetic experiments that attempt to model systematic errors in the data (such as those in Section 7). Therefore, to investigate the precision and accuracy of the estimated coefficients, the estimated covariance matrices must be supplemented with a variety of different tools. Nevertheless, valuable information derives from observations of how variances, covariance, and matrix condition change as a function of regression inputs. In this section we summarize our experience and provide guidelines for performing GSF regressions.

4.1 Diversity of events in GSF regressions

The number of distinct seismograms employed in GSF is important in determining the number of interaction coefficients that can be retrieved and reported with reasonable confidence. The signal in each seismogram is determined by the source and receiver vectors of equation (4). For a multiplet of degree ℓ, all of the information about the Earth from a single event is contained in the $2\ell+1$ time series $e^{i\mathbf{Z}t} \cdot \mathcal{S}$. Irrespective of how many receivers

sample these time series, for realistic signal-to-noise levels, $2\ell + 1$ time series are inadequate to determine much about the structure of the Earth. Thus, the retrieval of information about structural degrees above about 4 requires the use of a multiplicity of events, each contributing $2\ell + 1$ time series. Normal mode investigations which employ data from only one or two strong events can usually obtain reliable estimates for only even degree interaction coefficients through degree 6 at most, as demonstrated by He and Tromp [1996].

The importance of event distribution is illustrated by Figures 7, 8, and 9, which display condition numbers, variances, and covariances for two sets of regressions. These regressions target the isolated multiplet ${}_1S_8$ and the group of coupled multiplets ${}_0T_{18}$-${}_0S_{17}$-${}_2S_{11}$. The ${}_1S_8$ regressions estimate the 92 interaction coefficients of the even degrees 0-12. The ${}_0T_{18}$-${}_0S_{17}$-${}_2S_{11}$ regressions estimate 264 even degree coefficients: self-coupled degrees 0-10 of ${}_0T_{18}$; degrees 0-14 of ${}_0S_{17}$; degrees 0-8 of 2s11; and degree 6 and 8 cross-coupled coefficients for ${}_0S_{17}$-${}_2S_{11}$. The trial regressions are performed with data sets comprising increasing numbers of records and events. The first several events included are those which provide the largest quantity of high SNR recordings: event 15, Macquarie Ridge, 5/23/89; event 29, Northern Bolivia, 6/9/94; event 30, Kurile Islands, 10/4/94; event 32, Northern Chile, 7/30/95.

The trends in Figure 7a track condition number as recordings and events are added to the data sets. Those of Figure 7b similarly track "root-mean-variance", a summary of the estimated variances which is defined by $\bar{\sigma} = \sqrt{\sum_j C_{jj}/J}$, where J is the number of degrees of freedom. Increasing the number of recordings for a single event is much less important than adding the same number of recordings from a different event. Furthermore, condition numbers and variances for regressions using data from the 2 or 3 largest events can be reduced by as much as an order of magnitude by the addition of data from a dozen or more smaller events. The use of the full data set gives condition numbers below 25. In our experience, this is an important threshold, because most regressions with larger condition numbers are insufficiently stable to yield reliable coefficient estimates.

Perhaps more significantly, adding data from multiple events strongly affects covariances. Figures 8a and 8b demonstrate this using root-mean-covariances, defined by $\bar{\sigma}_j = \sqrt{\sum_{i \neq j} C_{ij}/(J-1)}$. The root-mean-covariances associated with the trial regressions of Figure 7 again imply that increasing the number of events has a greater impact than increasing the number of records from the few largest events. For both sets of regressions, use of the full

data set reduces overall covariance by about an order of magnitude relative to the covariances of regressions employing only the strongest three events. Just as importantly, the covariance matrices of the regressions become more diagonal and increasingly sparse as the data sets are expanded. Figure 9 demonstrates this effect using estimated covariance matrices normalized according to:

$$C'_{ij} = \frac{C_{ij}}{(C_{ii}C_{jj})^{1/2}} . \tag{10}$$

4.2 Interpreting Covariances

There are several notable characteristics of the estimated covariance matrices. The first is that sparseness is increased when events are added. The second relates to the nature of the covariances. With data from 3 large events, there is considerable covariance among all estimated self-coupled coefficients for ${}_1S_8$. This implies that, for ${}_1S_8$ and similar multiplets, the results of using limited data to estimate degrees 0-4 or 0-6 can be significantly biased by unconstrained structures at higher degrees. The experiments of Ritzwoller and Resovsky [1995a] confirm this.

Finally, even when a large number of events are employed, several significant covariances remain. The banded structure evident in the right-most matrices of Figure 9 indicate three dominant types of covariance that may be effectively irreducible:

(1) covariances between coefficients of the same multiplet and angular order (s) with azimuthal orders t and t' differing by 2;

(2) covariances between coefficients of a single multiplet with s and s' differing by 2 or 4;

(3) covariances between coefficients with identical structural indices ((s,t) = (s',t')) from the two Coriolis-coupled multiplets.

These covariances motivate further expansion of the data set, but may indicate that the distributions of large earthquakes and current seismographic stations are not adequate to resolve tradeoffs between estimates of the covarying coefficients.

The covariances between coefficients with different structural degrees also suggest that structures of degrees above those estimated are most likely to bias the highest 2 degrees of coefficient estimates for each multiplet. To test this hypothesis, we have constructed a

test model incorporating structure through degree and order 36. GSF was applied to the synthetic data to retrieve coefficients for the degrees estimated in the real data regression. The input and output coefficients from this experiment are compared in Table 2 and referred to as Experiment 1. While the estimates correlate well with the input model, the output coefficients at the highest degrees are amplified by 20-100% It is therefore advisable, and our practice, to discard at least the highest degree coefficients estimated for each multiplet or coupling pair. Thus, if we report coefficients to degree and order 10, regressions have been specified at least to 12 and preferably to 14 for that multiplet. Exceptions occur for fullly specified multiplets such as ${}_4S_3$, which is sensitive only to degrees 0-6, or for multiplets such as ${}_0S_4$ which are only weakly sensitive to aspherical structure.

4.3 Variable specification

There are not, in general, sufficient data to permit well-conditioned regressions for all of the interaction coefficients which affect the multiplets studied here. For each spectral window, only a subset of relevant interaction coefficients are specified as variables. The choice of which coefficients are specified is guided by experiments with synthetics and data. These experiments identify coefficients likely to be expressed in the data, and covariances that indicate potential sources of bias. The variables specified in each regression include as many as possible of the coefficients which affect the data. Particular emphasis is placed on including coefficients which would bias the estimates if not specified.

An example of variable specification is provided by the multiplet group ${}_3S_6$-${}_0T_{18}$-${}_1S_{12}$-${}_0S_{17}$-${}_2S_{11}$, all of which have degenerate frequencies within the same 25 μHz frequency band. Referring to the structural kernels of Figure 12, ${}_3S_6$ is most sensitive to the lower mantle, ${}_0S_{17}$ samples the transition zone, and ${}_0T_{18}$ and ${}_2S_{11}$ are upper mantle multiplets. ${}_1S_{12}$ is a CMB Stonely multiplet and is almost unobservable at the surface. Figure 10a displays synthetic spectra that demonstrate that all of the other multiplets should contribute significantly to the data. Figure 10b shows synthetics which typify the expected affects of the cross-coupled coefficients of pairs ${}_0T_{18}$-${}_0S_{17}$, ${}_0T_{18}$-${}_2S_{11}$, and ${}_0S_{17}$-${}_2S_{11}$. The effect of the ${}_0S_{17}$-${}_2S_{11}$ cross-coupling is nearly as large as that of the Coriolis coupling between the fundamentals. For many synthetics, the impact of the ${}_0T_{18}$-${}_0S_{17}$ coupling coefficients is also noticeable, but is small enough that it should be obscured by noise in most spectra. ${}_3S_6$ has a much higher Q

than the other multiplets and does not couple significantly to the others.

Inspection of the covariance matrix of Figure 9f indicates that there are significant covariances between ${}_0T_{18}$ and ${}_0S_{17}$ and between the self- and cross-coupled coefficients of ${}_0S_{17}$-${}_2S_{11}$. Other experiments reveal weak covariances between the cross-coupling of ${}_0T_{18}$-${}_0S_{17}$ and ${}_0T_{18}$-${}_2S_{11}$ and other coefficients, and almost no covariance between ${}_3S_6$ and the other multiplets. These observations imply that GSF need not be significantly biased if ${}_3S_6$ is analyzed apart from the other multiplets. Ignoring the ${}_0T_{18}$-${}_0S_{17}$ or ${}_0T_{18}$-${}_2S_{11}$ couplings should only slightly bias results for the other coefficients, but coupling between ${}_0S_{17}$-${}_2S_{11}$ should be specified in the regression.

These observations motivate GSF regressions for the self-coupled coefficients of ${}_3S_6$, ${}_0T_{18}$, ${}_0S_{17}$, and ${}_2S_{11}$, and for the cross-coupled coefficients of ${}_0S_{17}$-${}_2S_{11}$. One or more of these multiplets are observable on spectra from approximately 1400 recordings, of which about half are vertical component seismograms. Investigations of regression matrix condition numbers suggest that, with these data, GSF regressions can provide stable estimates for 300 coefficients, at most. Specifying coefficients for degrees 0-6 of ${}_3S_6$, degrees 0-8 of ${}_2S_{11}$, degrees 0-10 of ${}_0T_{18}$, degrees 0-14 of ${}_0S_{17}$, and degrees 6 and 8 of ${}_0S_{17}$-${}_2S_{11}$ requires a total of 293 variables. Because of the weak covariances between ${}_3S_6$ and the other multiplets, we choose to perform separate regressions for the 264 coefficients of ${}_0T_{18}$-${}_0S_{17}$-${}_2S_{11}$, using ~ 1200 recordings, and for the 29 ${}_3S_6$ coefficients with ~ 200 records. This separation is discussed further in the next subsection.

4.4 Data subsetting, windowing, and weighting

The choice of time series windows, events, and channels used in each regression depends on the nature of the modes targeted for analysis. For simplicity, a single time window is applied to all records in each regression for a given multiplet group. In general, time series windows begin a few hours after the event time, to permit the inclusion of gravimeter data and other records which are clipped immediately after large events. To enhance the signal-to-noise content in the data, the windows are as long as possible while insuring that the free oscillations remain above noise levels throughout most of the records employed.

Figure 11 illustrates the effective use both of different events and time windows to separate the signals of overlapping multiplets ${}_3S_6$ and ${}_0T_{18}$. Interference from strongly attenuated

modes like ${}_0T_{18}$ can be greatly reduced by employing time series beginning 10-15 hours after the events. Interference from upper mantle toroidal overtones is further reduced by employing only data from deep events recorded by vertically oriented instruments.

Ritzwoller *et al.* [1988] discussed the necessity of including weights in the regression matrices of SF. These regressions can be very sensitive to statistical outliers such as those produced by erroneous instrument response functions. Also, both SF and GSF preferentially fit data from the strongest events, which tends to moderate the benefits of using data from numerous events.

The weighting employed by Ritzwoller *et al.* [1988] addressed each of these concerns. For each data spectrum (index j) in each iteration of GSF, the RMS residual is $\sqrt{v_j} = [\sum_{i=1}^{I}(\Delta s_j(\omega_i))^2/I]^{1/2}$, where v_j is the variance of the residual. Both anomalous data and high-amplitude spectra tend to produce large RMS residuals when compared to synthetics. For this reason, each spectrum was weighted according to $w_j = 1/\sqrt{v_j}$, which both reduced sensitivity to outliers and de-emphasized data from strong events.

For GSF regressions, we have found it useful to modify these weights according to

$$\mathtt{w} = \frac{f^\beta}{\sqrt{v}}, \tag{11}$$

where $f = 1 - [v/\sum_i s^2_{\mathtt{data}}(\omega_i)]^{1/2}$ is the fractional RMS misfit. This modification serves to further deemphasize anomalous or low SNR records. In practice, values for β range from 0.25 to 2.0. Also, in order to avoid assigning excessively high weights to extremely high SNR records from recent large events, we cap the weights at some small factor (≤ 10) of the median of $1/\sqrt{v_j}$.

5 Results of GSF: Coefficient Estimates and Fits to Data

We have analyzed a total of 90 multiplets below 3 mHz of which 59 are spheroidal and 31 are toroidal. These multiplets and the maximum degree of the interaction coefficients estimated are shown in Figure 1. Self-coupled interaction coefficients for each of these multiplets are listed in Tables 5a-d. Thirteen spheroidal - toroidal pairs are coupled through the Coriolis force (${}_0S_9 - {}_0T_{10}$ to ${}_0S_{21} - {}_0T_{22}$) and thirteen multiplets are coupled through aspherical structure. Estimates of the interaction coefficients for cross-coupling are listed in Tables 5e-i.

For a regression to be considered converged, we have required that the coefficients estimated in the last three successive iterations at each degree correlate with better than 99% confidence, and their RMS amplitudes differ by less than 1%. Thus, reported estimates at each degree must demonstrate convergence in both amplitude and geometry. The only damping applied to the regressions is singular value truncation, which occurs for all singular values λ such that $\lambda_{max}/\lambda > 20$. Estimates are not reported when truncation is required for more than 5% of the singular values. The convergence of the estimates is not, therefore, a consequence of strong damping.

The characteristics of each regression are summarized by Tables 3a and 3b. Estimates of degenerate frequencies and Q's, and their uncertainties, are contained in Table 4. Tables 5a and 5b list the interaction coefficient estimates through degree 8, and corresponding uncertainties are in Tables 6a and 6b. Figure 12 displays a sampling of the generalized splitting function maps that result from our coefficient estimates. For comparison, each splitting function is displayed with a prediction from one of two models, SH.10c.17 or S12_WM13.

An important factor to consider in assessing the quality of the estimated coefficients is misfit. There are two separate contributors to misfit: additive noise, which to a fair approximation can be considered Gaussian, and theoretical errors which are not additive to the data. Theoretical errors include errors in nominal instrument responses, in moment tensor estimates, in the coupling scheme used, in the interaction coefficients used to construct the synthetics, and higher degree structures unspecified in the regression.

To quantify misfit in the spectral bands used to analyze each multiplet group, we employ a misfit ratio (MR). This quantity is defined by

$$\mathrm{MR} = \left(\frac{\sum_{i=1}^{I} \left[(s(\omega_i) - s'(\omega_i) \right]^2}{\sum_{i=1}^{I} s^2(\omega_i)} \right), \tag{12}$$

where $s(\omega_i)$ is the data spectrum for a given record and $s'(\omega_i)$ is the corresponding synthetic spectrum, computed with be estimated interaction coefficients. Phase and amplitude contributions to the misfit are examined separately, using phase misfit and amplitude misfit. Phase misfit is the average, across the frequency band analyzed, of the difference between the phases of the data and synthetic spectra. Amplitude misfit is the average of the difference between unity and the ratio of the amplitude of the synthetic to that of the data.

MR, phase misfits, and amplitude misfits that result from additive noise are expected to

decrese monotonically and asymptotically to zero with increasing signal-to-noise ratio (SNR) in the data. Figure 13 demonstrates this behavior with the results of a simulation, in which only additive noise was added to synthetic spectra for the coupled pair ${}_0S_{12} - {}_0T_{13}$. Least-squares-fit quadratic curves, constrained to have zero slope at high SNR, are overplotted. This figure may be constrasted with Figure 14, which displays the misfit plots for real data for the coupled trio ${}_0T_{18} - {}_0S_{17} - 2S_{11}$. Misfits observed for the real data vary with SNR in a manner consistent with the behavior of additive noise, except that at high SNR misfits level off at non-zero values. Such non-zero high SNR asymptotes are the expected signature of theoretical errors.

In constructing figures such as Figures 13 and 14, the noise level is estimated for each time series in our data set (station:channel:event) using the RMS amplitude averaged over a set of low frequency (0.5 - 2 mHz) spectral bands which are devoid of normal mode peaks. On vertical records there are 4 such bands (1.261 - 1.335, 1.435 - 1.480, 1.895 - 1.940, 2.605 - 2.645 mHz) and on horiztonal records there are 5 bands (1.265 - 1.305, 1.445 - 1.470, 1.886 - 1.915, 3.029 - 3.054, 3.125 - 3.150 mHz). The signal level is defined as the (1-norm) peak amplitude in the spectral window which contains the targeted multiplet or group of multiplets. SNR is simply the ratio of these estimates of signal and noise. Improved instrumentation and the very strong events of the past several years permit us now to characterize misfits for many records with extremely high SNR.

In Table 3b, the fit to the data given by the estimated interaction coefficients is compared to the fits produced by predictions from aspherical mantle models. Four misfit statistics are included: (1) MR averaged over all records used in each regression, (2) the high signal-to-noise ratio (HSNR) misfit which is the HSNR asymptotic value of the quadratic curve fit to MR versus log(SNR), (3) the HSNR amplitude misfit, and (4) the HSNR phase misfit. For poorly excited multiplets the HSNR misfits can be difficult to estimate accurately, and care has been taken to insure that the reported misfits are robust. Figure 15 displays the asymptotic trends that provide the HSNR statistics for 3 multiplets. In estimating HSNR asymptotes, it is assumed that these trends have zero slope above SNR= 70. When the distribution of SNR in the data does not extend to SNR= 70, best-fit trends which extrapolate to zero slope at SNR= 70 are employed whenever such fits prove robust.

Mean misfits and HSNR misfits provide significantly different information about the

regression. Mean misfits are related, but are not identical, to what is being minimized in each regression. They are also strong functions of the average SNR of the data set used. Consequently, mean misfits cannot meaningfully be compared between multiplets or across different data sets, since the noise contents for different multiplets or different data sets may differ. Comparisons of mean misfits resulting from different coefficient sets for the same multiplet group with the same data set are meaningful, however, and are included in Table 3b.

HSNR misfits are also included in Table 3b. These are generally more useful statistics since they estimate quantities that should be largely independent of SNR. They also provide estimates of the impact on the data of theoretical errors, which should be the dominant cause of errors in the estimated coefficients. For this reason, the HSNR misfits are the basis of the error analysis described in Section 7.

6 Assessing Interaction Coefficient Estimates

Providing an accurate assessment of the quality of estimates of normal mode interaction coefficients is as important as providing the coefficients themselves. We break assessment into two categories: qualitative and quantitative. Quantitative assessment is presented in terms of coefficient uncertainties and is discussed in Section 7. Qualitative assessment is the subject of this section.

6.1 Necessary Criteria for Reliable Coefficient Estimates

Experience with both simulated and real data shows that the following criteria should be met for the estimated interaction coefficients to be considered sufficiently accurate to be reported here.

- Estimated interaction coefficients should improve average and high SNR fit to the data relative to the coefficients obtained from regressions which estimate less detailed structures (lower degrees, less coupling).
- Estimated interaction coefficients should be consistent with the coefficients from multiplets with similar sensitivities to mantle structures. (Internal consistency.)

- Estimated interaction coefficients should fit data better than the coefficients predicted from recent mantle models, but should be consistent with these coefficients, especially in geographical distribution. (External consistency.)

6.2 Improvement of fit with higher structural degrees and coupling

With the addition of the high quality data recorded in the 1990's, inclusion of structural degrees above 4 significantly improves fit to the data. This has been discussed already by Ritzwoller and Resovsky [1995] and is further documented by the mean and HSNR misfits listed in Table 7. The HSNR misfits are most relevant to this issue since they are more useful in identifying theoretical errors such as the impact of higher degree structures on the data. Inclusion of Coriolis and structural coupling among all overlapping multiplets, in general, has an even more significant effect on data misfit than higher structural degrees.

6.3 Internal consistency

A useful check of the internal consistency of the estimated interaction coefficients is the correlation of the coefficients along an overtone branch, because modal sensitivity to earth structure tends to vary smoothly along each branch (with certain known exceptions). The thick solid lines in Figure 16 plot the confidence of the geographical correlation between the estimated coefficients for multiplets of adjacent l values along several modal branches. Estimated interaction coefficients along the overtone branches at the structural degrees reported are frequently correlated at better than 95% confidence, and are almost everywhere above the 90% confidence level. Exceptions are greatest when strong coupling occurs between pairs (e.g., ${}_1S_5 - {}_2S_4$, ${}_1S_6 - {}_2S_5$) or trios of multiplets (e.g., ${}_0T_{12} - {}_0S_{11} - {}_2S_7$, ${}_0T_{15} - {}_0S_{14} - {}_2S_9$, and ${}_0T_{18} - {}_0S_{17} - {}_2S_{11}$). Reported coefficients exhibiting relatively weak along-branch correlations are generally assigned larger uncertainties. It is important to note that the interaction coefficient estimates were made without employing any along-branch smoothness constraints.

6.4 Improvement of fit relative to existing models and external consistency

An example of a broadband spectrum displaying misfits for estimated and model interaction coefficients has been shown in Figure 2. In addition to providing misfit statistics for the

estimated coefficients, Table 3b lists the misfits for the coefficients predicted from either S12_WM13 or SH.10c.17, depending upon which model fits the data better for the specified mode group. In nearly every case, the estimated interaction coefficients provide better fits to the normal mode multiplets than the predictions of either model both in an averaged sense and for the highest SNR data in both amplitude and phase. Preliminary investigations suggest that the newer mantle models MK12_WM13 , S16B30, and SAW12D probably fit the these spectra no better than the older models S12_WM13 or SH.10c.17. Figure 15 illustrates the difference between the misfits for our coefficients and those predicted by S12_WM13 and SH.10c.17 for several multiplets. This figure and Table 3b demonstrate the improvement in fit to the data provided by the new coefficient estimates relative to model predictions. The coefficient estimates do, in general, fit both phase and amplitude data better than the models, although the relative size of these two differences varies considerably from one multiplet to another.

Figure 16 also presents correlations between the estimated coefficients and model predictions. The most important characteristic of these plots is that the GSF estimates usually correlate with at least one model better than the models correlate with each other. Thus, while the new normal modal coefficients and model predictions differ substantially, they are not inconsistent with what is presently believed about the Earth's interior structure.

Figure 17 identifies the primary difference between model predictions and the GSF interaction coefficients. These plots show the root-mean-squared (RMS) amplitude of the coefficients as a function of structural degree for both the models and our estimates. While both predicted and measured interaction coefficients are largest at degree 2, the estimates are consistently larger than predicted coefficients at degrees 4, 6, and 8 of structure, especially for the ${}_0T$ and ${}_2S$ modes which are dominantly sensitive to the upper mantle and transition zone. This implies a somewhat flatter, or whiter, spectrum of heterogeneity within these regions of the Earth than anticipated by the models. A possible source of the discrepancy may be the scalings between perturbations in ρ, v_s, and v_p, which are implicit in the construction of most of the models, and which may not be accurate if heterogeneities of different scale lengths have different causes.

7 Assigning Uncertainties

Ritzwoller *et al* [1988] showed that in spectral fitting, standard error analyses based on estimating the covariance matrix of the estimated coefficients provide uncertainty estimates that underestimate real errors in the coefficients. This proves to be true both for SF analyses of genuinely isolated multiplets and for GSF regressions. The reason is that the main sources of errors in the estimated coefficients are what was referred to in Section 5 as 'theoretical errors', which introduce systematic errors into the estimated coefficients. As discussed in Section 5, likely sources of systematic error include incorrect instrument responses, inaccurate source solutions, mantle structures of smaller scales than the estimated degrees, and other unspecified structures such as 3-D anelasticity and anisotropy. Ideally, these systematic errors should be identified by synthesizing each of the sources of error and estimating their impacts on the results of the regressions. However, there exists considerable ambiguity concerning the size and distribution of several of the unmodeled structures which render this process both highly inexact and time consuming. It is more effective and efficient to employ observed characteristics of the misfits obtained with the estimated coefficients to assess the net cumulative impact of these theoretical errors. Our approach is to estimate the effects of theoretical errors on the data in a statistical sense and to use this information to ascertain the expected affect of these errors on the data.

In Section 5, we discussed a model of the effect of additive noise and theoretical errors on normal mode spectra. For seismogram j and multiplet k this can be represented mathematically as follows:

$$
\begin{aligned}
{}_k s_j^{\mathbf{data}}(\omega) \;&\approx\; {}_k s_j^{\mathbf{synth}}(\omega) = < n_j(\omega) > + < {}_k A_j(\omega) > e^{i<{}_k\phi_j(\omega)>} {}_k s_j^{\mathbf{model}}(\omega) \qquad (13)\\
&=\; < n_j(\omega) > + < {}_k T_j(\omega) > {}_k s_j^{\mathbf{model}}(\omega). \qquad (14)
\end{aligned}
$$

The brackets <> stand for the 'expected value' of the enclosed quantity. In this model, theoretical errors are represented as a random process that is dependent on the multiplet, station, channel and event. This process imparts a frequency dependent modification to the amplitude and phase of the model seismogram, ${}_k s_j^{\mathbf{model}}(\omega)$, which can be represented as a complex transfer function, $< {}_k T_j(\omega) >$. For obvious reasons, we refer to this transfer function as 'multiplicative noise'. If the statistical characteristics of ${}_k T_j(\omega)$ can be ascertained, equation (14) can be used to simulate the effects of theoretical errors on the data that should match the statistics of misfit.

7.1 Simulating $< n(\omega) >$ and $< T(\omega) >$

The method used to estimate the additive noise level is discussed in Section 5. For simplicity, we assume that additive noise is frequency independent for each seismogram, which is a fairly good approximation for the frequency band considered here ($f < 3$ mHz). Good estimates of the theoretical noise transfer function are more difficult to obtain since it varies with the multiplet analyzed. To make progress we have found it useful to make the following assumptions. First, the frequency dependence of the theoretical noise is determined exclusively by the multiplet. That is, $< {}_kT_j(\omega) >$ is independent of frequency within a given multiplet and varies across the spectrum depending exclusively on which multiplet or multiplets occupy a spectral window. Synthetic experiments show that this should be a very good approximation in most cases for the frequencies considered here. Second, the expected value of ${}_kT_j(\omega)$ is independent of the recording index j. That is, it is independent of receiver location and event. This implies that expected errors in instrument responses are independent of station and that errors in estimates of moment tensors and event locations are independent of earthquake. It also implies that unmodeled structures are expected to have the same magnitude of affect on each recording independent of the location of the seismograph. This approximation is more troublesome. Detailed inspection of misfits indicate that it is not obviously a bad approximation, and without a much more extensive study of each of the sources of error, it is the best we can currently do. However, future work needs to be done to investigate the geographical coherence of the misfits.

With these approximations, the expected value of additive noise is just a function of the seismogram index j and the expected value of multiplicative noise is just dependent on the multiplet index k, and equation (14) can be rewritten as:

$$ {}_ks_j^{\mathbf{data}}(\omega) \approx {}_ks_j^{\mathbf{synth}}(\omega) =< n_j > + < T_k > {}_ks_j^{\mathbf{model}}(\omega). \tag{15} $$

The HSNR misfit in amplitude and phase discussed in Section 5 provides an estimate of $< T_k >$. An example of the absolute values of these quantities is plotted in Figure 14 for one set of coupled modes. In this case the expected HSNR asymptotic value of the phase error is about 6 degrees and the expected value of the amplitude error is about 11 percent. A histogram of the misfit in phase and amplitude for high SNR recordings (SNR > 75) for the same multiplet group is shown in Figure 18. Assuming that the amplitude and phase terms are both Gaussian around the mean of the distribution in Figure 18 with the observed

standard deviation, allows us to simulate $< T_k >$ for this multiplet group. One simulation of the random variable $< T_k >$ for the same set of records is also shown in Figure 18.

Using this statistical characterization of $< T_k >$ and adding random additive noise at the measured SNR for each recording in the data set for ${}_0T_{18} -_0 S_{17} -_2 S_{11}$, produces synthetic seismograms as shown in Figure 19 and the misfits between noise-free and the noisy synthetics shown in Figure 20. The same records are used in Figure 20 as in regressions with real data, except misfits here represent the difference between synthetics with and without noise (additive and multiplicative). Inspection of Figure 19 and comparing Figures 14 and 20 demonstrate that the gross characteristics of the data and misfits are reasonably well duplicated by the synthetics with additive and multiplicative noise of the form given by equation (15).

7.2 Monte-Carlo uncertainty estimates

Synthetic data with additive and multiplicative noise, as described in the previous subsection, can be used to assess the impacts of theoretical errors on interaction coefficient estimates. After a set of interaction coefficients have been estimated with GSF for a multiplet or group of multiplets, synthetic data are constructed for each seismogram and contaminated by the expected additive ($< n_j >$) and multiplicative ($< T_k >$) noise following equation (15). GSF is then applied to these noisy synthetics, and the estimated coefficients are compared with the input coefficients. A comparison between the input and estimated coefficients for one realization of the additive and multiplicative noise for ${}_0T_{18} -_0 S_{17} -_2 S_{11}$ is listed in Table 2 under Experiment 2. This simulation demonstrates that contamination by this noise degrades the amplitudes much more than the geometries of the coefficient estimates, and that the amplitudes are uniformly biased high especially for the highest degree estimated. This result is consistent with the synthetic experiment that simulated biasing due to higher degree structures and is the reason we have specified each regression to at least one degree higher than reported in Table 5.

This procedure is repeated for several realizations of the synthesized noise. The absolute value of the biases in each coefficient are averaged at each degree and order for each multiplet to yield the assigned uncertainties for the coefficient estimates. Thus, this is a Monte-Carlo error estimation procedure. We believe that this procedure produces the most robust error

estimates currently available for normal mode interaction coefficients.

8 Conclusions

The preceding sections have presented the application of Generalized Spectral Fitting (GSF) to the normal mode multiplets with frequencies below 3 mHz. GSF is a straightforward extension of the classical Spectral Fitting (SF) method [e.g., Ritzwoller *et al.*, 1988] that explicitly incorporates multiplet cross-coupling through aspherical struture and the Coriolis force in the estimation of normal mode interaction coefficients (elsewhere referred to as structure coefficients or splitting function coefficients). This allows many multiplets to be analyzed that could not be studied with SF because of strong coupling to other modes. Since spectra are more accurately fit with GSF, coefficients can now be estimated to structural degrees much higher than 4 and constraints can be placed on odd degree structures. The estimated interaction coefficients meet reasonable standards of internal consistency and misfit reduction and are externally consistent with existing mantle models, especially in geographical distribution. The coefficients have been assigned uncertainties which reflect the statistics of misfit. Taken together, these results should make the interaction coefficient estimates presented here generally much more useful than earlier published coefficients.

The development of GSF and its application in this paper have the following implications for future work:

- The new interaction coefficient estimates are complementary to body and surface wave data. In particular, they can be used to assess and refine models of 3-D mantle structure that are derived from other types of data.
- It should be practical to continue to apply GSF systematically at frequencies above 3 mHz. GSF may be particularly useful in modeling the elastic focusing and defocusing of long-period surface waves expressed through the cross-coupling of groups of 3, 5, or more adjacent multiplets along the fundamental mode branches.
- Because GSF can accurately model the amplitude effects of multiplet cross-coupling, it should extendable to estimate interaction coefficients for aspherical anelastic and anisotropic structures.

References

Dahlen, F. A., The spectra of unresolved split normal mode multiplets, *Geophys. J. R. Astron. Soc.*, **58**, 1-33, 1979.

Davis, J. P., Variation in apparent attenuation of the Earth's normal modes due to lateral heterogeneity, *Geophys. Res. Lett.*, **12**, 141-143, 1985.

Davis, J. P., Local eigenfrequency and its uncertainty inferred from spheroidal mode frequency shifts, *Geophys. J. R. Astron. Soc.*, **88**, 693-722, 1987.

Dziewonski, A. M. and D. L. Anderson, Preliminary Reference Earth Model, *Phys. Earth Planet. Int.*, **25**, 297-356, 1981.

Eckhardt, D. H., Correlations between global features of terrestrial fields, *Mathematical Geology*, **16**, 155-171, 1984.

Giardini, D., X. Li and J. H. Woodhouse, Three dimensional structure of the Earth from splitting in free oscillation spectra, *Nature*, **325**, 405-411, 1987.

Giardini, D., X.-D. Li and J. H. Woodhouse, The splitting functions of long period normal modes of the Earth, *J. Geophys. Res.*, **93**, 13,716-13,742, 1988.

Gilbert, F., Ranking and winnowing of gross earth data for inversion and resolution, *Geophys. J. R. Astron. Soc.*, **23**, 125-128, 1971.

Gilbert, F. and A. M. Dziewonski, An application of normal mode theory to the retrieval of structural parameters and source mechanisms from seismic spectra, *Philos. Trans. R. Soc. London, Ser. A*, **278**, 187-269, 1975.

He, X. , and J. Tromp, Normal-mode constraints on the structure of the Earth *J. Geophys. Res.*, 101, 20,053-20,082, 1996.

Jordan, T. H., A procedure for estimating lateral variations from low-frequency eigenspectra data, *Geophys. J. R. Astron. Soc.*, **52**, 441-455, 1978.

Lawson, C., and R. Hanson, *Solving Least Squares Problems*, Prentice Hall, Englewood Cliffs, N.J., 1974

Li, X.-D., and B. Romanowicz, Global mantle shear-velocity model developed using nonlinear asymptotic cou-

pling theory, submitted to *J. Geophys. Res.*, January, 1996.

Li, X.-D., D. Giardini, and J. H. Woodhouse, Large-scale three-dimensional even-degree structure of the Earth from splitting of long-period normal modes, *J. Geophys. Res.*, **96**, 551-557, 1991.

Masters, G. and F. Gilbert, Attenuation in the Earth at low frequencies, *Philos. Trans. R. Soc. London, Ser. A*, **308**, 479-522, 1983.

Masters, G. and M. H. Ritzwoller, Low frequency seismology and three dimensional structure: Observational aspects, in *Mathematical Geophysics, A survey of recent developments in seismology and geodynamics*, edited by N. J. Vlaar, G. Nolet, M. J. R. Wortel, and S. A. P. L. Cloetingh, Reidel Publ., Cordrecht, the Netherlands, 1987.

Masters, G., T. H. Jordan, P. G. Silver and F. Gilbert, Aspherical earth structure from fundamental spheroidal mode data, *Nature*, **298**, 609-613, 1982.

Masters, G., J. Park and F. Gilbert, Observations of coupled spheroidal and toroidal modes, *J. Geophys. Res.*, **88**, 10285-10298, 1983.

Masters, G., H. Bolton, and P. Shearer, Large-scale 3-dimensional structure of the mantle, *EOS, Trans. Am. Geophys. Un.*, **73**, 201, 1992.

Masters, G., S. Johnson, G. Laske, and H. Bolton, A shear-velocity model of the mantle, *Phil. Trans. R. Soc. Lond. A*, **354**, 1385 - 1411, 1996.

Park, J., Synthetic seismograms from coupled free oscillations: Effects of lateral structure and rotation, *J. Geophys. Res.*, **91**, 6441-6464, 1986.

Park, J. and F. Gilbert, Coupled free oscillations of an aspherical, dissipative, rotating Earth: Galerkin theory, *J. Geophys. Res.*, **91**, 7241-7260, 1986.

Resovsky, J. S. and M. H. Ritzwoller, Characterizing the long-period seismic effects of long-wavelength elastic and anelastic models, *Geophys. J. Internatl.*, **117**, 365 - 393, 1994.

Resovsky, J. and M. H. Ritzwoller, Constraining odd-degree mantle structure with normal modes, *Geophys. Res. Letts.*, **22**, 2301-2304, 1995a.

Resovsky, J.S. and M.H. Ritzwoller, Structural constraints and implications from an expanded set of mantle-sensitive normal modes, *EOS Trans. Am. Geophys. Un.*, F423, 1995b.

Ritzwoller, M.H. and E.M. Lavely, Three-dimensional seismic models of the Earth's mantle, *Revs. of Geophys.*, **33**, 1-66, 1995.

Ritzwoller, M. H., and J. Resovsky, The feasibility of normal mode constraints on higher degree structures, *Geophys. Res. Letts.*, **22**, 2305-2308, 1995.

Ritzwoller, M.H. and J. Wahr, Geodynamically consistent seismic inversion for mantle structure and internal boundary topography, *1994 Fall AGU Meeting, EOS Trans. Am. Geophys. Un.*, **75**, 663, 1994.

Ritzwoller, M.H. and J. Wahr, Normal mode constraints on mantle structure and dynamics, *IUGG XXI General Assembly*, B396, 1995. (INVITED)

Ritzwoller, M. H., G. Masters and F. Gilbert, Observations of anomalous splitting and their interpretation in terms of aspherical structure, *J. Geophys. Res.* **91**, 10203-10228, 1986.

Ritzwoller, M. H., G. Masters and F. Gilbert, Constraining aspherical structure with low harmonic degree interaction coefficients: Application to uncoupled multiplets, *J. Geophys. Res.*, **93**, 6269-6396, 1988.

Silver, P. G. and T. H. Jordan, Fundamental spheroidal mode observations of aspherical heterogeneity, *Geophys. J. R. Astron. Soc.*, **64**, 605-634, 1981.

Smith, M. F., and G. Masters, Aspherical structure constraints from normal mode frequency and attentuation measurements, *J. Geophys. Res.*, **94**, 1953-1976, 1989a.

Smith, M. F., and G. Masters, The effect of Coriolis coupling of free oscillation multiplets on the determination of aspherical earth structure, *Geophys. Res. Lett.* , **16**, 263-266, 1989b.

Su, W-J., and A. M. Dziewonski, Degree 12 model of shear velocity heterogeneity in the mantle, *J. Geophys. Res.*, **99**, 6945-6980, 1994.

Su, W-J., and A. M. Dziewonski, Simultaneous for 3-D variations in shear and bulk velocity in the mantle, submitted to *PEPI*, November, 1995.

Tromp, J., Support for anisotropy of the Earth's inner core, *Nature* , **366**, 678-681, 1993.

Tromp, J., Normal-mode splitting due to inner core anisotropy, *Geophys. J. Internatl.* , **121**, 963-968, 1995.

Tromp, J., and E. Zanzerkia, Toroidal splitting observations from the great 1994 Bolivia and Kuril Islands earthquakes, *Geophys. Res. Lett.* , **22**, 2297-3000, 1995.

Widmer, R., G. Masters, and F. Gilbert, Spherically symmetric attenuation within the Earth from normal mode data, *Geophys. J. Internatl.* , **104**, 541-553, 1991.

Widmer, R., W. Zurn, and G. Masters, Observations of low-order toroidal modes from the 1989 Macquarie Rise event, *Geophys. J. Internatl.* , **104**, 226-236, 1992a.

Widmer, R., G. Masters, and F. Gilbert, Observably split multiplets - data analysis and interpretation in terms of large-scale aspherical structure, *Geophys. J. Internatl.* , **111**, 559-576, 1992b.

Woodhouse, J. H., The coupling and attenuation of nearly resonant multiplets in the earth's free oscillation spectrum, *Geophys. J. R. Astron. Soc.*, **61**, 261-283, 1980.

Woodhouse, J. H. and F. A. Dahlen, The effect of a general aspherical perturbation on the free oscillations of the Earth, *Geophys. J. R. Astron. Soc.*, **53**, 335-354, 1978.

Woodhouse, J. H. and T. P. Girnius, Surface waves and free oscillations in a regionalized Earth model, *Geophys. J. R. Astron. Soc.*, **68**, 653-673, 1982.

Woodhouse, J. H., D. Giardini and X. D. Li, Evidence for inner core anisotropy from free oscillations, *Geophys. Res. Lett.*, **13**, 1549-1552, 1986.

Table and Figure Captions

Table 1: Summary of the data. Moments and depths are from the Harvard CMT catalogue. The stations providing data include vertical component gravimeters of the IDA network, and 3-component seismometers of the GDSN, GEOSCOPE and GSN networks.

Table 2: Measurements of interaction coefficient biasing in synthetic experiments. Comparison are between the "input" interaction coefficients used to construct synthetic data, and the "output" coefficients estimated using those data. Experiment 1 tests the effect of higher degree biasing. Synthetics are noise-free, but employ coefficients through degree 36 from a test model. Experiment 2 synthetics employ only coefficients at the estimated degrees, but incorporate both additive and multiplication noise at the observed levels (Section 5). Correlation confidence levels ("conf") are computed as in Figure 3. "RMS diff" is the root-mean-squared average of the difference between corresponding input and output interaction coefficients at each degree.

Table 3: (a) Summary of the data and ineteraction coefficients estimated with GSF. "nearby" multiplets are those which had to be explicitly included in regressions for the target multiplets. Letters in parentheses indicate which, if any, cross-coupled coefficients are estmated. For trios of multplets, "a" refers to the coupling of the first and second, and "c" to the coupling of the second and third. (b) Misfit statistics for the GSF regressions. Section 5 describes the average and asymptotic ("HSNR") misfit ratio ("MR") statistics. HSNR misfits are not reported when there are insufficient high SNR data to permit robust estimates of the asymptotes. The model misfits given for each regression are for the predicted interaction coefficients from S12_WM13 or SH.10c.17, whichever fits the data best. All synthetics employ GSF estimates of multiplet degenerate frequency and Q.

Table 4: GSF estimates of degenerate frequencies and Q's for normal mode multiplets below 3 mHz. These are equivalent to degree $s = 0$ complex interaction coefficients.

Table 5: GSF estimates of interaction coefficients for normal mode multiplets. Tables (a)-(d) give estimates for the interaction coefficients of self-coupling. Tables (e)-(i) give estimates for those of cross-coupling. Units are μHz. Only $t \geq 0$ coefficients are listed. The reality condition implies that for $t < 0$, $c_s^t = (-1)^{|t|} c_s^{|t|*}$. These coefficients may be compared to those normalized as in He and Tromp [1996], using the relations: $A_s^t = (-1)^t \sqrt{2\pi}\mathrm{Re}(c_s^t)$ and $B_s^t = (-1)^{t+1}\sqrt{2\pi}\mathrm{Im}(c_s^t)$ [Li *et al.*, 1991].

Table 6: HSNR misfit statistics illustrating the impact of estimates of interaction coefficients for coupling and for structures of degrees > 4. Misfits to data for synthetics that do not employ these coefficients (left column of each pair) are compared to misfits for synthetics that do employ the full sets of reported GSF estimates for each multiplet and coupling pair (right columns).

Figure 1: Dispersion diagrams displaying the multiplets analyzed in this study. The type of symbol indicates the maximum degree of interaction coefficient reported for each multiplet.

Figure 2: Sample comparisons of low-frequency normal mode spectra of data and synthetic seismograms. (a) Data amplitude spectrum from the IDA station ALE in Alert, Northwest Territories, after the deep Bolivian event of June 6, 1994, and the spectrum predicted by the recent Harvard model MK12_WM13. (b) The amplitude of the difference between these two complex spectra. In this example, which is typical of high signal-to-noise records, many multiplet peaks are misfit by more than 20%. (c) The amplitude of the difference between the data and a synthetic spectrum constructed using the interaction coefficients reported here. The largest residual amplitudes in this case are nearer to the 10% level.

Figure 3: Intermodel correlations for two generations of mantle models expressed in terms of confidence levels (Confidence is related to geographical correlation by Eckhardt [1984]). Models S12_WM13 and MK12_WM13 are from Harvard. Models SH.10c.17 and S16B30 are from Scripps Institution of Oceanography. Only the shear-velocity components of the models are compared. Persistent decorrelations between the two families of models are most pronounced in the transition zone and top of the lower mantle.

Figure 4. Input and estimated interaction coefficients for a synthetic experiment. This demonstrates the bias caused by Coriolis coupling of coefficients estimated without accounting for the coupling.

Figure 5: Geographical distribution of the data set employed. There has been a marked increase in the number of events and stations employed compared to those in Ritzwoller *et al.* (1988).

Figure 6: Example of editing to produce reliable data. The large glitches in the original time series produce a large DC offset and considerable noise in the spectrum. When these are removed by editing, overtone peaks, such as the lower mantle ${}_5S$ multiplets, become observable.

Figure 7: (a) Matrix condition numbers of the singular-value-decompositions of GSF for a series of regressions employing increasing numbers of stations and events to estimate interaction coefficients of ${}_1S_8$ and of ${}_0T_{18} - {}_0S_{17} - {}_2S_{11}$. The horizontal axis gives the number of records used and labels indicate the events

which provide each set of addtional records. Event numbers refer to Table 1. (b) Root-mean-variances for each of these regressions. The circled numbers and letters mark regressions selected for the plots of Figure 8.

Figure 8: Root mean covariances, as functions of variable index, for several of the regressions of Figure 7, for (a) ${}_1S_8$ and (b) ${}_0T_{18} - {}_0 S_{17} - {}_2 S_{11}$. The multiplets are ordered as indicated, with coefficient degree increasing from left to right.

Figure 9: The normalized covariance matrices for several of the the regressions of the sequence shown in Figure 7. The darker boxes indicate matrix elements with larger amplitudes. (a), (b), and (c) show even degrees 0-12 of ${}_1S_8$, ordered left-to-right and top-to-bottom starting with real and imaginary parts of degree 0. In (d), (e), and (f), covariances for the self-coupling of ${}_2S_{11}$ are in the upper left, followed by those for ${}_0T_{18}$ and ${}_0S_{17}$. Covariances among the cross-coupling coefficients of ${}_0S_{17}$-${}_2S_{11}$ are in the lower right corner.

Figure 10: (a) Sample spectra illustrating the effect of overtones beneath a pair of fundamental multiplet peaks. The inclusion of ${}_2S_{11}$ and its coupling to ${}_0S_{17}$ through aspherical structure of degrees $s = 6, 8$ improves fit to the peak on the right. The peak on the left is fit better when ${}_3S_6$ is included. The time window here is intermediate between those which best accentuate the individual multiplets. (b) Sample spectra illustrating the relative impacts of the various couplings of ${}_0T_{18} - {}_0 S_{17} - {}_2 S_{11}$. The Coriolis coupling of ${}_0T_{18} - {}_0 S_{17}$ and interaction coefficients for the structural coupling between ${}_0S_{17} - {}_2 S_{11}$ have the greatest impacts.

Figure 11: An example illustrating the use of selected time windows and events to enhance observations of particular multiplets. Each plot shows synthetic spectra created using the ${}_3S_6$ and ${}_0T_{18} - {}_0 S_{17} - {}_2 S_{11}$ interaction coefficient sets both separately and together. The spectra of long, late-starting time series from the deep Bolivian event are dominated by ${}_3S_6$ while shorter timeseries for the shallow Kurile event yield spectra dominated by ${}_0T_{18}$ in the same frequency band.

Figure 12: Generalized splitting functions from GSF estimates of self-coupling and cross-coupling interaction coefficients. Also displayed are the splitting functions predicted by mantle models SH.10c.17 or S12_WM13, and normalized kernels indicating the sensitivities of the multiplets to v_s (solid) and v_p (dashed) structures as functions of depth. In general, multiplets with similar sensitivities are observed to have similar splitting functions, and observations resemble model predictions, though the amplitudes of the observed coefficients are often noticeably greater at degrees above $s = 4$. ${}_6S_3$ exhibits an anomalous splitting function typical of multiplets sensitive to core anisotropy [*e. g.* Woodhouse, *et al.*, 1986; Tromp, 1993,

1995].

Figure 13: Simulated variation with SNR of the misfit between noise-free synthetics and synthetics contaminated by additive noise. Misfit ratio (MR), amplitude misfit, and phase misfit are defined in Section 5. "Noise-free" synthetics employ only model S16B30 predictions of ${}_0T_{18} - {}_0S_{17} - {}_2S_{11}$ interaction coefficients. For "noisy" synthetics, the "noise-free" synthetics are perturbed at each frequency by additive noise of random phase with RMS amplitude matching the observed SNR of each record. The "best fit" trends shown result from a least-squares fit to the median of the distribution which employs a quadratic [in log(SNR)] between SNR=3 and SNR=70, and a horizontal line [asymptote] above SNR=70.

Figure 14: Variation of misfit with SNR in GSF residuals. Residuals are from a comparison of the data subset employed in the analysis of ${}_0T_{18} - {}_0S_{17} - {}_2S_{11}$ to synthetics computed using the reported interaction coefficients for these multiplets. The "best fit" trends are computed as in Figure 13.

Figure 15: Sample quadratic trends in MR for the isolated multiplets ${}_1S_8$ and ${}_5S_6$ and the Coriolis-coupled pair ${}_0T_{13} - {}_0S_{12}$. Such curves are used in constructing Table 3b.

Figure 16: Correlation confidence levels for internal and external consistency checks of the GSF coefficient estimates. The along-branch trends compare estimated interaction coefficients of adjacent multiplets on the same overtone branch. Also shown are the correlations of the estimates to either SH.10c.17 or S12_WM13, whichever agrees better with the measurements. Correlations between these two models are displayed for comparison.

Figure 17: RMS amplitude of the observed interaction coefficients at each degree of structure. The amplitudes are normalized by the degenerate frequencies of the multiplets. Amplitudes predicted by models SH.10c.17 and S12_WM13 are also shown.

Figure 18: Distribution of amplitude and phase misfits for spectra of ${}_0T_{18} - {}_0S_{17} - {}_2S_{11}$ with SNR$>$ 50. Residuals are for (solid) data compared to synthetics made using the observed interaction coefficients and (dotted) synthesized data of appropriate additive noise levels and multiplicative noise distributions compared to noise-free synthesized data. The multiplicative noise distributions appear to be adequately duplicated in this realization.

Figure 19: Comparison of data spectra and noisy synthetic spectra (additive and multiplicative) for several SNR levels for the multiplet trio ${}_0T_{18} - {}_0S_{17} - {}_2S_{11}$.

Figure 20: Simulated variation of misfit with SNR. This figure is contructed similarly to Figure 14, except that the "noisy" data include multiplicative noise as well as additive noise. The multiplicative noise is distributed as in Figure 19. The synthesized misfit trends figures compare favorably with those observed in Figure 15, although the misfit values in this simulation are somewhat less scattered than in the real data.

Table 1: data summary

index	date	(Julian)	location	depth (km)	moment (10^{20}Nm)	stations providing useful data
1	6/22/77	(173)	Tonga	61	13.9	14
2	8/19/77	(231)	S. of Sumbawa	23	35.9	17
3	12/6/78	(340)	Kuril Is.	181	6.4	24
4	12/12/79	(346)	Ecuador Coast	20	16.9	25
5	7/17/80	(199)	Santa Cruz Is.	34	4.8	25
6	6/22/82	(173)	Banda Sea	473	1.7	33
7	3/28/83	(077)	New Ireland	70	4.6	33
8	11/20/84	(325)	Mindanao	181	2.2	42
9	3/3/85	(062)	Central Chile	41	10.3	39
10	9/19/85	(262)	Michoacan	21	11.0	45
11	5/7/86	(127)	Andreanof Is.	31	10.4	52
12	10/20/86	(293)	Kermadec Is.	50	4.5	50
13	11/30/87	(334)	Gulf of Alaska	15	7.3	52
14	3/16/88	(066)	Gulf of Alaska	15	4.9	53
15	5/23/89	(143)	Macquarie Is.	15	13.6	62
16	3/3/90	(062)	S. of Fiji	25	3.0	53
17	4/18/90	(108)	Minahassa	33	3.3	64
18	7/16/90	(197)	Luzon	15	4.1	60
19	12/30/90	(364)	New Britian	205	1.8	62
20	4/22/91	(112)	Costa Rica	15	3.3	69
21	9/2/92	(246)	Nicaragua	15	3.4	70
22	10/11/92	(285)	Vanuatu	141	1.5	69
23	12/12/92	(347)	Flores Is.	20	5.1	78
24	1/15/93	(015)	Hokkaido	100	2.7	68
25	7/12/93	(193)	Hokkaido	17	4.7	82
26	8/8/93	(220)	S. of Mariana	59	5.2	76
27	3/9/94	(068)	Fiji Is.	567	3.1	82
28	6/2/94	(153)	S. of Java	15	5.3	44
29	6/9/94	(160)	North Bolivia	647	26.3	88
30	10/4/94	(277)	Kuril Is.	68	30.0	76
31	12/28/94	(362)	E. of Honshu	34	4.0	46[a]
32	7/30/95	(211)	Northern Chile	20	16.8	63[a]
33	10/9/95	(282)	Jalisco	49	11.5	42[a]
34	12/3/95	(337)	Kuril Is.	22	8.2	10[a]
35	1/1/96	(001)	Minahassa	33	7.8	10[a]
36	2/17/96	(048)	West Irian	33	24.1	10[a]
37	6/17/96	(169)	Flores Sea	593	5.2	10[a]

[a]data processing incomplete

Table 2: synthetic bias

multiplet	degree	Exp. # 1, out vs in		Exp. # 2, out vs in	
(n type l)	(s)	% corr. confid.	ratio of rms amp	% corr. confid.	ratio of rms amp
0 T 18	2	99.99	0.952	99.99	0.976
	4	99.99	0.918	99.99	1.121
	6	99.99	1.095	99.99	0.899
	8	99.99	0.966	99.54	1.635
	10	99.99	1.638	98.43	2.802
0 S 17	2	99.99	1.009	99.99	1.003
	4	99.99	1.106	99.99	0.973
	6	99.99	1.070	99.99	1.067
	8	99.99	1.215	99.99	1.118
	10	99.99	1.034	99.99	1.306
	12	99.99	1.276	99.80	1.473
	14	99.56	2.034	98.22	1.880
2 S 11	2	99.99	1.087	99.99	1.058
	4	99.99	0.996	99.99	0.931
	6	99.99	1.113	99.99	1.239
	8	99.99	1.264	99.97	1.457
0 S 17	6	99.99	0.973	99.99	1.108
2 S 11	8	99.99	1.180	99.99	1.050

Table 3a: Regression Inputs

target multipets	nearby multiplets	number events	number horizontal	number vertical	number variables	highest degrees estimated
${}_0S_4$	-	16	4	182	46	8
${}_0S_5$	-	23	9	345	46	8
${}_0S_6$	-	25	57	495	46	8
${}_0S_7,{}_2S_3$	${}_0T_7,{}_1T_1$	18	0	287	46	8,6
${}_0S_8$	${}_4S_1,{}_0T_9$	32	57	553	67	10
${}_0S_9$-${}_0T_{10}$	${}_1T_4$	32	50	550	92	8,8
${}_0S_{10}$-${}_0T_{11}$ (a)	${}_4S_2$	32	528	1036	172	14,8,(2)
${}_0T_{12}$-${}_0S_{11}$-${}_2S_7$ (a,b,c)	-	33	512	1018	233	8,12,8,(2,6,6)
${}_0T_{13}$-${}_0S_{12}$	${}_6S_1$	24	450	855	246	12,16
${}_0T_{14}$-${}_0S_{13}$	${}_5S_2,{}_1T_7$	24	450	855	246	12,16
${}_0T_{15}$-${}_2S_9$-${}_2T_2$-${}_0S_{14}$ (e)	-	33	508	992	293	10,8,14,8,(7)
${}_0T_{16}$-${}_0S_{15}$	-	33	521	1063	246	12,16
${}_0T_{17}$-${}_0S_{16}$	${}_1T_9$	33	511	1027	246	12,16
${}_0T_{18}$-${}_0S_{17}$-${}_2S_{11}$ (a,c)	${}_3S_6$	24	404	736	269	10,14,8,(2,8)
${}_0T_{19}$-${}_0S_{18}$	${}_3S_7,{}_5S_5$	24	407	762	246	12,16
${}_0T_{20}$-${}_0S_{19}$ (a)	-	33	459	948	215	10,14,(6)
${}_0S_{20}$-${}_0T_{21}$-${}_2S_{13}$ (a)	${}_8S_1,{}_2T_8$	25	292	681	239	14,10,8(2)
${}_0S_21$	${}_1S_14,{}_0T_22,{}_5S_6$	25	0	634	154	16
${}_1S_2$	-	4	2	24	16	4
${}_1S_3$-${}_3S_1$ (a)	${}_0T_5$	17	0	256	50	6,2,(4)
${}_1S_4$	-	15	12	160	46	8
${}_1S_5$-${}_2S_4$ (a)	${}_0T_8$	23	137	455	149	10,8,(7)
${}_2S_5$-${}_1S_6$ (a)	-	16	86	181	128	8,8,(7)
${}_1S_7$	-	16	1	210	46	8
${}_1S_8$	-	20	0	284	92	12
${}_1S_9$	-	12	1	118	46	8
${}_1S_{10}$	-	12	1	85	46	8
${}_1S_14$	${}_0S_21,{}_0T_22,{}_5S_6$	8	82	212	16	4
${}_2S_6$	-	18	155	169	67	10
${}_2S_8$	${}_4S_3$	20	167	370	46	8
${}_2S_{10},{}_4S_5$	-	20	143	301	92	8,8
${}_3S_2$	-	10	0	90	16	4
${}_3S_6$	${}_0T_{18}$-${}_0S_{17}$-${}_2S_{11}$	2	68	93	29	6
${}_3S_7,{}_5S_5$	${}_0T_{19}$-${}_0S_{18}$	17	7	215	80	6,8
${}_3S_8$-${}_6S_3$ (a)	-	22	91	233	101	8,6,(7)
${}_4S_1$	${}_0S_8$	2	12	66	7	2
${}_4S_2$	${}_0S_{10}$-${}_0T_{11}$	2	64	113	16	4
${}_4S_3$	${}_2S_8$	20	96	357	29	6
${}_4S_4$-${}_1T_8$ (a)	-	16	102	163	84	6,6,(7)
${}_5S_2$	${}_0T_{14}$-${}_0S_{13},{}_1T_7$	2	0	104	7	2
${}_5S_3$	-	19	120	185	29	6
${}_5S_4$-${}_2T_4$ (a)	-	22	61	391	111	8,6,(7)
${}_6S_1$	${}_0T_{13}$-${}_0S_{12}$	2	61	113	7	2
${}_8S_1$	${}_0S_20$-${}_0T_21$-${}_2S_13$	5	0	132	7	2
${}_0T_4$	-	3	17	0	7	2
${}_0T_5$	${}_1S_3$-${}_3S_1$	4	66	0	46	8
${}_0T_6$	-	16	151	0	29	6
${}_0T_7,{}_1T_1$	${}_0S_7,{}_2S_3$	5	104	0	36	6,2
${}_0T_8$	${}_1S_5$-${}_2S_4$	12	151	0	29	6
${}_0T_9$	${}_0S_8,{}_2S_5$-${}_1S_6$	13	205	0	29	6
${}_0T_{22}$	${}_1S_14,{}_0S_21,{}_5S_6$	24	286	0	67	10
${}_1T_2$	-	2	66	0	7	2
${}_1T_3$	-	2	81	0	7	2
${}_1T_4$	${}_0S_9,{}_0T_10$	9	49	0	16	4
${}_1T_5$	${}_0S_10$-${}_0T_11$	14	388	0	29	6
${}_1T_6$	-	14	176	0	46	8
${}_1T_7$	${}_5S_2,{}_0T_14$-${}_0S_13$	22	417	0	29	6
${}_1T_9$	${}_0T_17$-${}_0S_16$	18	462	0	29	6
${}_2T_8$	${}_0S_20$-${}_0T_21$-${}_2S_13$	12	283	0	29	6

Table 3b: Regression fits

target multipets	mean misfit		HSNR misfit		amp. misfit (%)		phase misfit (°)	
	model	GSF	model	GSF	model	GSF	model	GSF
${}_0S_4$	.49	.47	.24	.20	13.0	12.6	7.0	6.2
${}_0S_5$	.42	.39	.16	.12	7.8	7.3	5.0	2.3
${}_0S_6$	.40	.36	.12	.09	5.7	4.5	4.0	2.5
${}_0S_{7,2}S_3$	.45	.37	.28	.13	8.0	5.1	7.8	3.6
${}_0S_8$	.42	.37	.25	.13	7.4	6.1	6.6	3.5
${}_0S_9$-${}_0T_{10}$	.47	.43	.24	.15	5.6	6.7	7.3	5.8
${}_0S_{10}$-${}_0T_{11}$	.52	.48	.27	.18	12.0	8.4	7.8	5.0
${}_0T_{12}$-${}_0S_{11}$-${}_2S_7$	.53	.51	.31	.21	10.4	8.7	8.1	4.8
${}_0T_{13}$-${}_0S_{12}$	.50	.45	.29	.24	13.3	11.0	8.6	7.0
${}_0T_{14}$-${}_0S_{13}$	.54	.49	.25	.19	11.1	8.9	8.7	5.7
${}_0T_{15}$-${}_0S_{14}$-${}_2S_9$	.56	.50	.32	.22	14.1	13.3	9.3	5.2
${}_0T_{16}$-${}_0S_{15}$	.55	.48	.33	.22	15.3	12.4	7.9	6.8
${}_0T_{17}$-${}_0S_{16}$	.58	.51	.35	.26	16.7	14.3	8.2	8.1
${}_0T_{18}$-${}_0S_{17}$-${}_2S_{11}$	.63	.48	.40	.24	19.4	10.8	10.2	6.2
${}_0T_{19}$-${}_0S_{18}$	.64	.59	.38	.28	21.0	16.8	11.4	6.2
${}_0T_{20}$-${}_0S_{19}$	.67	.59	.40	.31	19.4	13.8	10.3	7.9
${}_0S_{20}$-${}_0T_{21}$-${}_2S_{13}$	.56	.49	.41	.31	16.7	13.6	9.3	6.6
${}_0S_{21}$	.60	.53	.39	.32	20.5	18.5	9.9	8.1
${}_1S_2$	.49	.47	-	-	-	-	-	-
${}_1S_3$-${}_3S_1$	.47	.45	.13	.09	3.4	5.1	4.5	5.6
${}_1S_4$	.46	.34	.17	.13	3.4	4.0	5.5	4.2
${}_1S_5$-${}_2S_4$	.58	.50	.22	.14	2.8	1.1	3.9	2.6
${}_2S_5$-${}_1S_6$	.47	.38	.24	.10	5.5	2.5	5.6	2.5
${}_1S_7$	.42	.35	.14	.07	2.8	3.2	3.7	2.3
${}_1S_8$	.49	.36	.22	.06	2.8	0.7	6.0	2.8
${}_1S_9$	.54	.42	.35	.13	6.3	1.8	13.2	2.8
${}_1S_{10}$	.57	.41	-	-	-	-	-	-
${}_1S_{14}$	.54	.54	.33	.31	13.1	13.6	8.2	8.2
${}_2S_6$	.45	.38	.21	.12	11.5	7.9	5.5	2.0
${}_2S_8$	.58	.45	.21	.14	6.2	6.6	6.5	4.9
${}_2S_{10,4}S_5$	.77	.71	.50	.41	24.4	29.7	12.4	9.5
${}_3S_2$	.89	.63	.25	.16	70.2	55.5	16.3	10.9
${}_3S_6$	.72	.62	.50	.46	22.8	15.3	10.5	16.4
${}_3S_7$-${}_5S_5$	.66	.46	.48	.19	9.8	3.8	9.8	5.6
${}_3S_8$-${}_6S_3$	.84	.43	.70	.10	45.6	6.1	29.0	5.6
${}_4S_1$	.44	.40	.27	.19	15.7	7.1	5.8	3.2
${}_4S_2$	.58	.49	.36	.19	16.6	13.0	15.3	6.7
${}_4S_3$	.75	.59	.42	.15	13.3	3.1	7.6	5.0
${}_4S_4$-${}_1T_8$	.60	.59	.38	.28	15.9	10.0	10.1	8.6
${}_5S_2$	.49	.51	.21	.20	13.0	14.4	4.3	6.8
${}_5S_3$	.71	.68	.45	.35	14.3	4.6	7.0	6.4
${}_5S_4$-${}_2T_4$	.68	.45	.53	.13	13.3	4.7	12.9	3.1
${}_6S_1$	.75	.59	.51	.33	23.1	15.9	15.3	8.8
${}_8S_1$	.77	.49	.47	.33	12.6	12.9	8.4	6.7
${}_0T_4$	.45	.40	-	-	-	-	-	-
${}_0T_5$	.44	.39	-	-	-	-	-	-
${}_0T_6$	.59	.57	.35	.28	18.0	12.2	3.8	8.1
${}_0T_{7,1}T_1$	.52	.47	.26	.15	7.2	5.9	3.4	2.2
${}_0T_8$	.59	.57	.28	.19	7.1	7.6	4.2	3.1
${}_0T_9$	.45	.42	.23	.15	11.1	4.2	5.8	3.7
${}_0T_{22}$	.70	.72	.44	.44	-	-	-	-
${}_1T_2$	.69	.69	-	-	-	-	-	-
${}_1T_3$	.56	.52	-	-	-	-	-	-
${}_1T_4$	.36	.35	.12	.12	3.4	1.0	2.8	5.3
${}_1T_5$	.57	.56	.14	.14	2.3	2.5	3.1	4.4
${}_1T_6$	.64	.56	.34	.27	11.2	9.3	11.4	10.9
${}_1T_7$	.49	.49	.19	.19	14.1	11.1	4.4	5.1
${}_1T_9$	.49	.48	.22	.20	11.2	12.9	8.5	8.1
${}_2T_8$	.64	.62	.44	.38	-	-	11.2	10.9

Table 4: multiplet degenerate frequency and Q estimates

mult.	ω (mHz)	$\omega - \omega_{PREM}$ μHz	Q	$Q - Q_{PREM}$
${}_0S_4$	0.64689	-0.20	370	-4
${}_0S_5$	0.84002	-0.42	360	4
${}_0S_6$	1.03753	-0.70	341	-7
${}_0S_7$	1.23103	-0.78	353	10
${}_0S_8$	1.41282	-0.70	346	8
${}_0S_9$	1.57763	-0.67	343	10
${}_0S_{10}$	1.72566	-0.82	335	7
${}_0S_{11}$	1.86124	-1.19	331	8
${}_0S_{12}$	1.98917	-1.22	328	13
${}_0S_{13}$	2.11165	-1.30	325	18
${}_0S_{14}$	2.23006	-1.36	318	20
${}_0S_{15}$	2.34450	-1.39	314	25
${}_0S_{16}$	2.45690	-1.32	306	27
${}_0S_{17}$	2.56615	-0.99	293	24
${}_0S_{18}$	2.67223	-1.08	288	29
${}_0S_{19}$	2.77615	-0.83	288	39
${}_0S_{20}$	2.87774	-0.64	280	39
${}_0S_{21}$	2.97725	-0.49	266	34
${}_0T_4$	0.76609	0.43	268	39
${}_0T_5$	0.92837	0.13	254	37
${}_0T_6$	1.07928	0.44	245	40
${}_0T_7$	1.22100	0.29	207	12
${}_0T_8$	1.35658	0.46	200	13
${}_0T_9$	1.48707	0.45	187	7
${}_0T_{10}$	1.61350	0.42	177	4
${}_0T_{11}$	1.73767	0.63	173	6
${}_0T_{12}$	1.85868	0.73	165	2
${}_0T_{13}$	1.97785	0.86	165	6
${}_0T_{14}$	2.09548	1.11	157	2
${}_0T_{15}$	2.21088	0.52	151	-1
${}_0T_{16}$	2.32628	1.08	149	-1
${}_0T_{17}$	2.44040	1.28	149	2
${}_0T_{18}$	2.55295	0.71	140	-5
${}_0T_{19}$	2.66565	0.93	142	-2
${}_0T_{20}$	2.77731	0.62	145	3
${}_0T_{21}$	2.88843	0.22	131	-10
${}_0T_{22}$	3.00026	0.86	130	-9
${}_1S_2$	0.68022	0.37	367	56
${}_1S_3$	0.94014	0.31	310	27
${}_1S_4$	1.17299	0.13	294	23
${}_1S_5$	1.37016	-0.12	331	39
${}_1S_6$	1.52147	-0.57	395	49
${}_1S_7$	1.65457	-0.95	423	51
${}_1S_8$	1.79793	-1.38	417	37
${}_1S_9$	1.96182	-1.94	423	42
${}_1S_{10}$	2.14598	-2.47	433	54
${}_1S_{14}$	2.97400	-1.82	306	13
${}_1T_1$	1.23568	-0.43	269	9
${}_1T_2$	1.31925	-0.86	295	38
${}_1T_3$	1.43833	-0.77	274	21
${}_1T_4$	1.58508	-0.41	292	42
${}_1T_5$	1.74996	-0.53	274	27
${}_1T_6$	1.92510	-0.51	263	20
${}_1T_7$	2.10312	-0.68	295	58
${}_1T_8$	2.27948	-0.77	270	38
${}_1T_9$	2.45233	-0.18	244	19
${}_2S_3$	1.24299	0.78	416	1
${}_2S_4$	1.37957	0.37	386	5
${}_2S_5$	1.51537	0.43	310	8
${}_2S_6$	1.68126	0.42	243	5
${}_2S_7$	1.86519	0.23	215	4
${}_2S_8$	2.04965	0.45	206	8
${}_2S_9$	2.22933	0.58	188	0
${}_2S_{10}$	2.40404	1.14	189	8
${}_2S_{11}$	2.57253	0.38	180	34
${}_2S_{13}$	2.89972	-0.09	174	-12
${}_2T_2$	2.23237	1.56	230	25
${}_2T_4$	2.37910	-0.73	238	28
${}_2T_8$	2.91236	-1.29	253	24
${}_3S_1$	0.94447	0.53	852	25
${}_3S_2$	1.10642	0.21	284	-82
${}_3S_6$	2.54884	-0.80	289	14
${}_3S_7$	2.68561	-0.72	279	10
${}_3S_8$	2.81931	-0.33	270	6
${}_4S_1$	1.41174	-0.89	364	9
${}_4S_2$	1.72162	-0.67	466	32
${}_4S_3$	2.04134	-0.83	528	47
${}_4S_4$	2.27821	-1.39	313	23
${}_4S_5$	2.41149	0.08	282	0
${}_5S_2$	2.09067	-0.61	322	4
${}_5S_3$	2.16928	-0.36	319	27
${}_5S_4$	2.37921	-0.31	554	65
${}_5S_5$	2.70357	0.22	570	67
${}_5S_6$	3.01138	0.69	589	83
${}_6S_1$	1.98417	3.78	298	-351
${}_6S_3$	2.82186	0.14	492	65
${}_8S_1$	2.87269	-0.67	973	44

Table 5a, degree 2 self-coupling interaction coefficient estimates

mult.	c_2^0	re c_2^1	im c_2^1	re c_2^2	im c_2^2
${}_0S_4$	1.44	0.28	0.30	-0.81	0.98
${}_0S_5$	1.76	0.52	0.34	-1.50	1.78
${}_0S_6$	1.77	0.75	0.43	-2.35	2.29
${}_0S_7$	0.57	1.04	0.33	-2.84	2.62
${}_0S_8$	1.50	1.36	0.47	-2.69	3.09
${}_0S_9$	1.09	1.53	0.28	-1.93	3.04
${}_0S_{10}$	-0.41	1.83	0.31	-2.02	3.80
${}_0S_{11}$	-3.15	2.83	0.38	-1.40	4.71
${}_0S_{12}$	-4.43	2.64	-0.07	-1.12	5.43
${}_0S_{13}$	-5.40	2.96	0.03	-0.41	5.84
${}_0S_{14}$	-6.72	2.99	-0.27	0.28	7.44
${}_0S_{15}$	-7.41	3.85	0.38	0.53	8.18
${}_0S_{16}$	-10.08	4.31	-0.38	0.97	9.34
${}_0S_{17}$	-9.45	4.78	-0.32	0.92	8.63
${}_0S_{18}$	-10.21	5.25	0.06	1.65	9.10
${}_0S_{19}$	-11.71	5.17	-0.09	3.48	11.14
${}_0S_{20}$	-11.12	5.64	-0.50	3.59	11.06
${}_0S_{21}$	-12.29	5.85	-1.35	3.96	12.18
${}_0T_4$	0.81	0.54	-0.77	-0.39	-0.31
${}_0T_5$	-1.46	0.51	0.62	-0.99	2.24
${}_0T_6$	-0.77	0.88	-0.42	-0.23	3.71
${}_0T_7$	-1.38	1.82	0.46	0.67	4.50
${}_0T_8$	-2.36	2.04	-0.03	1.58	4.64
${}_0T_9$	-0.45	2.46	-1.56	2.17	6.15
${}_0T_{10}$	2.84	2.73	-0.21	3.22	7.58
${}_0T_{11}$	1.36	2.57	-1.16	3.62	7.81
${}_0T_{12}$	-1.07	3.83	-1.83	4.74	8.41
${}_0T_{13}$	-4.12	2.37	-2.27	4.74	11.21
${}_0T_{14}$	-1.92	3.23	-2.44	5.02	10.06
${}_0T_{15}$	-3.42	2.48	-6.13	6.28	12.23
${}_0T_{16}$	-7.52	4.64	-7.17	9.84	12.94
${}_0T_{17}$	-3.61	6.62	-4.76	7.80	12.18
${}_0T_{18}$	0.22	4.89	-6.41	12.15	15.59
${}_0T_{19}$	-2.13	5.08	-6.70	9.98	14.40
${}_0T_{20}$	4.46	8.24	7.37	9.92	16.42
${}_0T_{21}$	4.85	6.94	-7.19	11.61	15.45
${}_0T_{22}$	-10.38	8.16	-7.39	11.62	24.55
${}_1S_2$	0.69	0.70	1.25	-0.67	0.45
${}_1S_3$	0.03	0.74	0.61	-1.38	2.26
${}_1S_4$	0.34	0.65	0.71	-1.93	2.60
${}_1S_5$	1.79	0.23	0.77	-3.28	3.24
${}_1S_6$	2.22	-0.38	0.33	-4.82	3.23
${}_1S_7$	3.54	0.28	0.96	-5.25	3.30
${}_1S_8$	5.00	0.26	0.71	-5.85	3.59

mult.	c_2^0	re c_2^1	im c_2^1	re c_2^2	im c_2^2
${}_1S_9$	6.04	0.47	0.29	-7.09	4.14
${}_1S_{10}$	8.22	0.03	2.22	-8.73	4.92
${}_1S_{14}$	15.59	6.13	2.68	-5.85	8.86
${}_1T_1$	4.23	-0.63	-1.72	-3.87	0.25
${}_1T_2$	-2.35	0.18	-0.53	0.36	1.48
${}_1T_3$	-0.40	0.29	0.80	-2.14	3.57
${}_1T_4$	0.64	1.34	0.69	-0.58	5.64
${}_1T_5$	1.53	0.47	0.08	-4.77	4.34
${}_1T_6$	1.42	-0.31	-0.11	-5.92	5.56
${}_1T_7$	4.64	3.03	4.34	-2.35	7.09
${}_1T_8$	1.73	1.08	1.13	-3.79	7.57
${}_1T_9$	7.05	1.58	1.49	-3.43	4.26
${}_2S_3$	8.53	0.40	0.23	-2.46	1.92
${}_2S_4$	1.36	1.18	0.48	-2.43	3.31
${}_2S_5$	-0.02	2.59	1.02	-1.28	4.36
${}_2S_6$	-2.68	3.59	1.36	0.72	6.94
${}_2S_7$	-4.26	3.89	2.88	0.19	8.17
${}_2S_8$	-4.60	5.07	1.98	1.89	9.30
${}_2S_9$	-4.47	5.73	2.34	3.70	11.77
${}_2S_{10}$	-2.65	5.44	3.27	2.25	11.09
${}_2S_{11}$	-3.48	6.43	3.92	2.80	14.07
${}_2S_{13}$	-3.78	6.09	4.84	0.78	17.69
${}_2T_2$	0.19	-0.21	1.45	0.64	2.26
${}_2T_4$	3.95	-0.03	3.28	-3.54	2.92
${}_2T_8$	8.36	0.47	1.96	-10.90	11.28
${}_3S_1$	0.43	-0.02	-0.19	-0.27	0.85
${}_3S_2$	13.64	0.99	-0.30	3.54	1.37
${}_3S_6$	3.52	1.61	2.17	-6.94	6.40
${}_3S_7$	-0.42	2.15	0.54	-7.31	10.81
${}_3S_8$	3.51	2.71	1.57	-4.54	8.99
${}_4S_1$	0.78	0.55	0.76	0.67	1.11
${}_4S_2$	-0.52	-0.22	0.34	0.24	1.15
${}_4S_3$	-0.52	-0.27	0.38	0.31	2.39
${}_4S_4$	0.08	-0.01	0.54	-4.07	1.91
${}_4S_5$	4.43	1.67	1.35	-5.22	7.15
${}_5S_2$	1.11	1.17	1.29	-0.52	3.90
${}_5S_3$	1.02	0.68	1.37	-2.79	3.85
${}_5S_4$	-0.49	0.35	0.68	-1.21	2.60
${}_5S_5$	0.37	0.45	1.03	-1.24	4.09
${}_5S_6$	0.56	0.43	1.43	-2.36	5.51
${}_6S_1$	11.41	4.01	7.58	-1.61	3.08
${}_6S_3$	16.38	-0.45	1.03	-1.55	3.82
${}_8S_1$	3.46	-1.02	0.75	-0.07	1.63

Table 5b, degree 4 self-coupling interaction coefficient estimates

mult.	c_4^0	re c_4^1	im c_4^1	re c_4^2	im c_4^2	re c_4^3	im c_4^3	re c_4^4	im c_4^4
${}_0S_5$	0.01	0.10	0.10	-0.02	0.00	-0.08	0.35	-0.06	-0.33
${}_0S_6$	-0.24	0.05	0.58	0.45	0.18	0.61	0.65	-0.04	-0.53
${}_0S_7$	-0.93	-0.06	0.25	0.11	0.16	0.25	0.11	0.15	-0.76
${}_0S_8$	0.78	0.23	0.55	0.55	0.33	0.92	0.90	0.38	-0.47
${}_0S_9$	-0.12	-0.23	-0.11	0.67	0.46	0.84	0.76	0.16	0.78
${}_0S_{10}$	-0.30	-0.10	0.29	0.43	0.04	1.53	1.25	1.35	-0.55
${}_0S_{11}$	0.55	-0.83	0.11	0.80	0.26	1.53	0.26	0.40	-1.65
${}_0S_{12}$	-1.16	-0.68	-0.31	1.14	-0.19	1.79	1.78	1.21	-1.17
${}_0S_{13}$	-0.77	-0.03	-0.37	1.25	0.46	2.94	1.71	0.44	-1.01
${}_0S_{14}$	1.06	1.03	-0.83	1.86	1.02	1.58	1.74	1.72	-1.79
${}_0S_{15}$	1.21	0.10	-0.31	2.08	1.31	1.46	1.63	0.25	-1.59
${}_0S_{16}$	2.06	1.21	-1.03	0.78	2.23	1.17	1.37	1.86	-2.16
${}_0S_{17}$	-1.13	-0.90	-0.72	1.51	1.01	1.73	1.66	0.31	-0.72
${}_0S_{18}$	2.33	-0.88	-1.34	1.52	1.79	1.28	1.58	-1.06	-1.08
${}_0S_{19}$	-1.87	-0.90	-0.43	1.27	1.51	2.32	1.19	1.41	-1.67
${}_0S_{20}$	1.15	-0.86	-0.67	0.81	1.00	1.12	1.37	0.07	-0.56
${}_0S_{21}$	-1.85	-0.08	-0.48	0.21	1.22	0.71	1.14	0.90	-0.39
${}_0T_5$	-0.47	-0.18	1.63	0.99	0.65	-0.78	0.94	1.06	0.01
${}_0T_6$	-0.12	0.89	0.50	-0.35	0.61	-0.08	0.38	0.05	-0.11
${}_0T_7$	1.77	2.02	-1.94	0.93	-0.36	1.15	-0.71	-0.46	-1.03
${}_0T_8$	0.34	1.43	-0.53	-0.97	-0.97	1.56	-0.36	0.09	-3.00
${}_0T_9$	2.83	0.32	-0.63	0.97	-3.07	1.95	-0.09	0.50	-3.49
${}_0T_{10}$	-2.60	0.06	-4.13	-0.03	0.25	1.35	0.76	0.49	-2.47
${}_0T_{11}$	1.10	2.17	-1.98	-1.55	-0.18	1.64	-0.14	-0.67	-3.79
${}_0T_{12}$	0.91	0.85	-0.96	-3.07	-1.84	2.13	1.38	0.07	-3.99
${}_0T_{13}$	4.23	1.50	-1.57	-4.38	-2.10	2.41	1.67	0.23	-5.18
${}_0T_{14}$	2.92	0.95	-0.66	-4.65	1.86	3.74	-0.07	1.29	-4.26
${}_0T_{15}$	5.37	1.19	2.19	0.22	-3.74	-1.07	1.86	-0.15	-4.87
${}_0T_{16}$	3.91	0.01	1.81	-2.97	-0.55	3.70	0.64	1.56	-9.40
${}_0T_{17}$	2.57	0.72	1.16	-3.97	-0.85	3.47	-0.40	-2.82	-5.35
${}_0T_{18}$	-1.48	1.59	0.10	-5.21	-2.68	4.09	0.06	0.50	-8.82
${}_0T_{19}$	11.40	-2.82	2.37	-4.26	-6.51	6.41	1.47	1.74	-7.23
${}_0T_{20}$	-5.21	4.25	-3.97	-8.91	-5.16	4.31	1.82	-0.13	-9.97
${}_0T_{21}$	3.00	3.94	-1.94	-4.50	-2.61	5.82	0.67	0.14	-11.90
${}_0T_{22}$	6.61	-2.55	7.51	6.78	0.96	12.56	0.77	6.40	-8.94
${}_1S_4$	-0.13	0.23	0.02	0.66	0.46	0.17	-0.10	0.94	0.00
${}_1S_5$	-0.44	0.61	-0.18	0.50	0.43	0.22	0.99	0.12	-0.06
${}_1S_6$	-0.87	0.94	-0.35	1.14	0.95	0.05	0.51	0.16	0.05
${}_1S_7$	-0.84	0.91	0.40	1.19	0.51	0.25	1.14	0.45	-0.19
${}_1S_8$	-0.85	1.08	0.21	1.59	0.85	0.09	0.93	0.24	-0.13
${}_1S_9$	-0.22	0.81	0.31	1.69	1.39	-0.27	0.86	-0.57	0.52
${}_1S_{10}$	-0.16	1.09	1.17	2.89	2.84	-1.71	1.35	0.30	1.47
${}_1T_4$	-1.03	-0.47	-0.15	3.03	0.41	-0.62	-1.04	0.74	-1.97
${}_1T_5$	-0.06	-0.18	0.29	-0.60	-1.49	1.77	0.54	-1.03	-0.41
${}_1T_6$	-0.34	0.44	0.28	0.18	-0.37	-1.34	2.85	-1.62	3.25
${}_1T_7$	-5.74	2.85	-1.37	0.72	-0.54	0.70	1.04	0.67	-3.02
${}_1T_8$	-2.76	2.12	0.38	-0.73	1.39	-2.88	-0.65	0.92	-3.62
${}_1T_9$	2.71	0.01	-1.41	1.07	-2.85	-0.21	0.13	0.91	-1.93
${}_2S_3$	0.22	0.40	0.21	0.89	-0.42	-0.67	0.12	-0.44	-0.74
${}_2S_4$	-0.45	0.16	0.44	0.45	0.12	0.17	0.62	-0.36	0.53
${}_2S_5$	0.52	0.68	0.81	-0.69	-1.45	0.34	0.46	0.16	-0.76
${}_2S_6$	0.45	0.21	-0.42	0.13	-0.85	0.83	0.65	0.44	-1.90
${}_2S_7$	1.47	0.83	0.67	-1.32	-0.98	1.25	0.98	-1.03	-2.09
${}_2S_8$	2.78	0.01	-0.17	-1.85	-1.03	0.40	-0.33	0.81	-2.70
${}_2S_9$	3.01	-0.17	0.34	-2.01	-0.79	0.76	-1.59	0.30	-4.39
${}_2S_{10}$	2.04	0.39	-2.83	-3.27	-2.53	-0.42	-0.02	-1.76	-5.24
${}_2S_{11}$	2.40	1.17	-2.71	-3.96	1.19	1.03	-0.22	1.42	4.78
${}_2S_{13}$	2.27	1.36	-1.93	6.08	1.86	2.52	0.01	-0.19	-8.44
${}_2T_4$	3.22	2.84	-2.71	0.90	0.34	-1.68	-0.56	-0.96	-1.59
${}_2T_8$	-4.71	3.19	-0.78	-0.26	1.08	0.55	1.31	0.84	-2.53
${}_3S_2$	0.10	1.21	0.31	5.11	0.84	0.15	0.22	0.62	-0.03
${}_3S_6$	0.09	1.73	-2.49	-0.16	2.91	-3.92	-3.48	-4.99	-0.87
${}_3S_7$	-0.93	-0.95	0.88	2.51	2.78	2.79	0.58	2.09	-1.63
${}_3S_8$	-1.02	-0.28	1.55	0.79	0.21	-0.16	-0.43	-2.01	-1.21
${}_4S_3$	-0.71	-0.34	-0.97	0.61	-1.03	-0.52	0.86	0.28	0.81
${}_4S_4$	0.36	-1.95	-1.74	0.81	2.80	2.80	4.55	-3.41	0.29
${}_4S_5$	-1.07	-1.15	-1.04	-0.55	0.97	-0.61	1.03	-0.80	-1.64
${}_5S_3$	0.14	-0.33	-0.95	0.50	0.03	0.31	1.42	-0.24	-1.06
${}_5S_4$	0.10	0.50	-0.38	-0.44	-1.52	0.24	0.81	-0.19	-0.52
${}_5S_5$	-0.73	1.13	-0.32	-0.68	0.77	-0.60	0.07	0.72	-1.15
${}_5S_6$	-0.75	1.47	-0.11	0.14	0.39	-1.19	-0.22	-0.27	-0.79
${}_6S_3$	5.34	0.94	-0.05	0.83	0.21	-1.16	0.43	0.75	0.37

Table 5c, degree 6 self-coupling interaction coefficient estimates

mult.	c_6^0	re c_6^1	im c_6^1	re c_6^2	im c_6^2	re c_6^3	im c_6^3	re c_6^4	im c_6^4	re c_6^5	im c_6^5	re c_6^6	im c_6^6
${}_0S_6$	-0.28	0.15	-0.07	0.03	-0.51	-0.23	0.39	0.03	-0.13	-0.05	0.14	0.29	-0.34
${}_0S_7$	-0.76	0.07	0.09	-1.03	0.03	0.31	0.10	0.08	0.15	-0.90	0.50	0.68	-0.46
${}_0S_8$	-0.06	-0.46	-0.30	-1.03	-0.26	-0.36	0.49	0.28	-0.55	-0.85	0.82	0.62	-0.50
${}_0S_9$	0.33	0.76	0.09	-1.22	-0.33	0.30	1.03	0.55	-0.55	-1.31	0.41	0.59	0.51
${}_0S_{10}$	0.67	0.91	-0.01	-1.56	-0.25	-0.22	0.86	-0.11	-0.95	-1.39	0.38	1.26	-0.12
${}_0S_{11}$	-1.73	1.10	-0.80	-2.06	0.79	1.61	0.83	-0.45	-0.56	-0.78	0.20	1.06	0.26
${}_0S_{12}$	-1.61	0.71	-0.10	-2.00	-0.83	-0.79	1.99	-0.41	-1.70	-1.33	-0.11	2.61	-0.06
${}_0S_{13}$	-0.83	1.34	0.93	1.66	-0.24	0.68	1.81	-1.74	-1.17	-1.25	-0.59	1.78	0.56
${}_0S_{14}$	-0.56	0.68	0.18	-1.57	1.05	-0.30	2.47	-1.23	-1.72	-1.25	0.32	2.05	-0.53
${}_0S_{15}$	2.33	2.53	1.02	-2.11	0.61	0.43	2.06	-1.76	-1.83	-1.76	0.27	1.49	0.33
${}_0S_{16}$	2.38	2.21	-0.60	-1.88	2.60	-1.06	2.77	-0.47	-1.42	-1.48	-0.39	0.83	-0.32
${}_0S_{17}$	-2.37	2.48	-0.53	-2.95	0.81	-0.28	2.05	-2.61	-1.86	-1.69	0.14	2.28	-0.92
${}_0S_{18}$	-4.93	1.78	-0.80	3.48	0.86	0.60	3.17	-2.63	-1.23	-3.08	-1.81	3.35	1.51
${}_0S_{19}$	-2.59	2.68	0.61	-2.54	0.12	0.44	1.31	-1.54	-2.79	-2.90	-1.86	1.84	0.71
${}_0S_{20}$	1.58	2.51	1.04	-2.60	0.46	0.22	2.14	-2.87	-2.30	-2.17	-1.15	1.02	0.09
${}_0S_{21}$	-2.85	2.72	0.04	-1.46	0.52	0.64	1.89	-3.08	-2.28	-1.23	1.42	0.59	-0.02
${}_0T_{10}$	1.02	1.42	1.20	-0.06	-0.46	0.85	1.75	0.99	-0.56	-0.16	0.07	0.97	-0.47
${}_0T_{11}$	-1.02	1.48	0.22	2.10	-1.22	0.11	2.16	-1.22	-1.28	-1.60	-0.24	1.81	-0.06
${}_0T_{12}$	0.61	2.12	-0.61	-1.04	-0.85	1.71	4.37	-0.36	-0.70	-2.30	0.90	2.34	-1.02
${}_0T_{13}$	-0.57	3.32	0.75	0.43	-1.06	1.60	4.23	-1.46	-1.43	-2.68	0.22	-1.88	0.64
${}_0T_{14}$	3.05	2.93	0.39	1.96	-0.97	-0.16	4.45	-2.06	-1.16	2.98	-1.50	-1.21	-3.06
${}_0T_{15}$	-2.43	8.88	0.34	5.74	-1.78	0.16	1.98	-2.91	-4.55	-3.23	4.39	2.14	2.03
${}_0T_{16}$	-2.12	5.43	-4.24	0.56	0.70	0.30	5.09	1.30	-3.74	-1.37	-0.40	1.40	0.97
${}_0T_{17}$	4.64	4.88	-3.94	-0.18	-3.69	1.03	2.53	2.39	-5.41	-8.19	1.60	3.57	-1.26
${}_0T_{18}$	2.59	5.62	-2.14	0.55	-3.07	4.31	6.46	-1.79	-6.82	-5.34	-0.47	-1.08	1.23
${}_0T_{19}$	-4.59	8.18	4.48	-5.49	-1.09	2.56	7.56	-1.35	-4.85	-7.23	0.32	0.92	-4.25
${}_0T_{20}$	11.29	8.87	5.43	-6.55	0.70	-0.32	7.41	-1.60	-5.83	-6.48	3.07	2.96	-4.53
${}_0T_{21}$	1.96	1.68	-2.29	-5.52	-3.69	0.03	9.25	-0.92	-3.76	-10.90	3.04	2.79	-1.19
${}_1S_6$	-0.15	0.25	-0.43	0.25	0.28	0.21	0.06	-0.39	0.19	-0.82	0.54	0.79	0.14
${}_1S_6$	0.64	0.28	-0.50	-0.36	-0.15	-0.47	-0.17	-0.46	-0.85	-1.07	0.09	0.87	-0.17
${}_1S_7$	0.81	0.68	-0.14	-0.87	-0.02	0.19	0.37	-0.14	-0.36	-0.19	0.47	0.05	0.57
${}_1S_8$	-0.39	0.37	0.70	-0.69	-0.28	-0.11	0.18	-0.34	-0.99	0.13	0.51	0.55	0.41
${}_1S_9$	-0.59	0.56	-1.10	-0.34	-1.00	-0.21	-0.63	-0.83	-1.46	-0.30	-0.14	0.14	0.24
${}_1T_8$	0.08	-0.01	-0.20	1.14	0.10	0.69	0.77	0.09	0.47	1.30	0.62	2.03	-0.15
${}_1T_9$	4.97	-1.90	0.35	-0.69	-0.27	-0.10	4.23	1.60	1.81	0.71	-2.10	1.30	0.13
${}_2S_3$	1.04	0.00	-1.58	-0.44	-0.02	0.36	0.10	0.10	-0.84	-0.37	1.06	-0.68	0.83
${}_2S_4$	-0.02	0.30	-0.35	-0.28	-0.36	0.70	-0.30	0.07	-0.41	-0.44	0.17	0.28	0.24
${}_2S_5$	0.05	0.41	0.18	0.26	-1.25	1.06	-0.67	-0.86	-1.63	-0.32	1.12	0.64	1.00
${}_2S_6$	-1.08	0.20	0.13	-0.75	-0.05	1.12	0.35	-1.05	-1.33	-0.99	0.78	0.64	-0.37
${}_2S_7$	2.14	1.00	0.02	0.58	-1.70	1.53	2.95	1.40	-2.57	-0.09	-0.15	1.65	1.25
${}_2S_8$	1.47	3.48	-0.77	-0.50	-0.23	1.42	2.58	-0.88	-1.07	-1.60	-0.75	3.31	0.19
${}_2S_9$	0.47	2.56	-1.26	0.39	1.12	0.30	4.16	-1.84	-0.22	-2.51	-0.15	3.16	-0.62
${}_2S_{10}$	1.70	2.30	-3.34	-3.22	0.28	-0.55	4.93	-1.57	-2.57	-2.63	1.87	2.17	0.41
${}_2S_{11}$	-0.53	4.26	-2.88	2.33	1.91	0.67	7.49	-2.29	3.16	-3.04	2.96	2.16	-2.58
${}_2S_{13}$	0.67	4.47	-0.90	-2.94	-2.42	2.13	7.31	-1.66	3.52	-5.26	0.75	1.94	-3.42
${}_3S_8$	1.85	1.76	-0.50	0.78	-1.50	0.04	1.19	1.39	-0.42	-1.51	2.83	0.32	0.94
${}_4S_3$	0.66	0.07	-1.85	0.96	-0.29	0.25	-1.24	0.33	-0.68	0.03	-0.28	0.20	-0.21
${}_5S_3$	1.25	0.01	-0.64	0.86	1.02	-0.38	-1.13	0.32	-0.36	-0.75	1.29	-0.38	0.93
${}_5S_4$	-0.38	0.18	-0.20	-0.19	0.19	-0.01	0.06	0.26	-0.80	-0.80	-0.63	-0.50	-0.03
${}_5S_5$	0.09	0.24	0.07	0.89	0.08	0.00	0.50	0.16	-0.11	0.22	-1.53	-0.09	0.00
${}_5S_6$	-0.12	0.44	0.48	0.02	0.94	0.98	0.77	-0.41	0.34	0.15	-1.13	0.48	0.82
${}_6S_3$	0.44	0.98	-0.61	-0.92	-0.26	-1.24	-1.00	0.48	0.41	0.34	1.07	-1.28	-0.32

Table 5d, degree 8 self-coupling interaction coefficient estimates

mult.	c_8^0	re c_8^1	im c_8^1	re c_8^2	im c_8^2	re c_8^3	im c_8^3	re c_8^4	im c_8^4	re c_8^5	im c_8^5	re c_8^6	im c_8^6	re c_8^7	im c_8^7	re c_8^8	im c_8^8
${}_0S_8$	0.48	-0.38	-0.23	-0.46	-0.08	-0.82	0.10	0.35	-0.73	-0.28	0.13	0.14	-0.01	0.36	0.06	0.50	-0.54
${}_0S_9$	0.47	-0.02	0.14	0.77	0.14	-0.26	-0.09	0.01	-0.11	0.03	0.06	-0.07	0.01	0.12	0.03	0.47	-0.08
${}_0S_{10}$	0.38	0.10	-0.47	-0.92	0.85	-0.12	-0.28	0.00	-0.12	0.22	-0.38	-0.30	-0.23	0.68	-0.06	0.28	-1.05
${}_0S_{11}$	-0.24	0.11	1.15	-2.14	0.44	1.88	0.59	-0.19	0.28	1.21	0.08	-0.41	-0.70	1.74	-1.12	-1.53	-0.40
${}_0S_{12}$	2.07	0.56	-0.46	0.50	-1.02	-0.95	-0.51	-0.36	1.77	0.03	-0.21	-1.09	1.14	0.92	-0.28	0.35	-1.95
${}_0S_{13}$	1.59	0.48	-0.62	1.79	-1.22	-0.09	-0.51	-0.27	-1.70	-0.75	0.48	-1.34	-0.70	0.86	-0.25	-0.84	-1.23
${}_0S_{14}$	0.03	0.40	0.74	-1.33	-0.07	0.27	0.13	-0.91	-1.49	0.05	-0.35	-0.77	-1.54	1.45	-0.62	0.53	-0.62
${}_0S_{15}$	0.04	1.28	-0.35	-1.00	-0.16	0.23	-0.41	-0.49	2.34	0.77	0.42	-2.21	-1.72	0.93	-0.65	0.10	-0.55
${}_0S_{16}$	0.13	0.38	-1.94	-1.94	0.31	0.14	0.01	0.56	-1.49	0.00	0.92	-2.69	-1.68	0.59	-1.16	0.02	-0.61
${}_0S_{17}$	0.19	1.13	-0.32	2.91	0.18	0.22	0.77	-1.47	-1.89	-0.49	0.03	-0.84	-1.13	1.10	0.88	0.06	-1.52
${}_0S_{18}$	-1.31	-1.29	-1.28	-3.17	0.04	-1.32	1.17	-2.94	-0.82	-0.63	1.14	0.60	-0.19	2.71	-0.15	0.99	-2.67
${}_0S_{19}$	0.26	1.47	1.29	-3.68	0.50	-0.08	0.37	-1.38	-3.01	0.91	0.32	-2.04	-1.38	2.55	-0.51	-0.75	-1.51
${}_0S_{20}$	0.46	1.80	0.97	-2.62	0.17	0.83	0.78	-1.84	-1.95	-0.09	0.19	-2.20	-1.70	0.14	-0.82	0.61	-3.47
${}_0S_{21}$	0.79	1.75	0.29	-2.81	-0.21	1.86	0.57	-3.03	1.98	0.81	0.16	-1.07	-2.48	0.46	1.81	0.64	-2.08
${}_0T_{10}$	0.25	0.44	0.14	0.30	0.14	-0.28	0.32	0.00	0.28	-0.70	0.20	0.15	0.26	0.32	0.46	0.00	-0.24
${}_0T_{16}$	5.32	3.94	3.44	-2.02	2.56	3.13	3.44	0.28	-1.21	-0.12	0.80	-2.88	-0.81	1.39	-1.57	2.03	2.52
${}_0T_{16}$	-1.30	6.02	1.15	-5.86	3.20	0.74	-3.44	-0.44	-0.50	-0.29	0.62	-1.17	-4.39	-0.21	-4.95	1.01	0.33
${}_0T_{17}$	-1.70	1.51	2.77	-4.21	-1.84	1.19	0.12	-2.78	-1.65	-2.19	2.63	2.78	-6.46	2.54	0.00	0.91	-2.12
${}_0T_{18}$	4.95	-0.19	0.57	-5.50	-0.04	1.70	0.43	0.13	4.09	0.12	-0.12	-4.45	-3.25	1.95	-2.56	1.49	-0.75
${}_0T_{19}$	2.01	3.93	2.26	5.24	-3.45	4.41	1.28	-3.74	-1.01	1.33	5.52	-6.26	-1.38	1.08	-0.09	0.42	-1.73
${}_0T_{20}$	7.42	-1.14	-5.13	-3.52	-3.71	3.70	1.19	-0.24	3.75	0.19	-0.72	1.63	-5.95	0.86	5.03	0.89	-0.02
${}_0T_{21}$	1.00	6.59	-5.20	-5.76	2.25	-1.30	1.14	-3.89	-2.83	-0.81	-0.67	-1.90	-1.39	0.82	-0.77	-1.02	0.82
${}_1S_7$	0.91	0.81	0.17	0.26	0.22	-0.81	0.15	0.88	-0.68	1.00	0.01	-0.56	-0.40	0.51	-0.05	1.18	0.38
${}_1S_8$	0.74	-0.48	0.37	0.10	-0.16	-0.45	-0.09	0.44	-0.74	-0.14	0.31	0.41	-0.26	0.20	0.85	1.80	-0.83
${}_1S_9$	0.72	-1.01	0.06	0.25	0.57	-1.61	-0.22	1.13	-0.22	-0.78	0.22	-0.54	0.14	-0.10	0.32	1.44	-1.65
${}_2S_{10}$	-1.50	0.44	0.59	-3.04	0.38	0.90	0.85	-1.52	-1.40	0.39	0.33	0.13	-0.65	-0.66	0.72	1.65	-1.00
${}_2S_{13}$	-0.58	-0.08	1.07	-1.95	-1.96	-0.87	1.34	-1.56	-3.99	0.45	1.37	-0.52	-3.18	-2.22	1.90	1.58	-1.74
${}_6S_4$	-0.04	0.17	0.02	0.03	-0.26	0.25	0.08	0.56	0.08	0.30	0.11	-0.01	0.39	-0.43	0.00	-0.38	-0.41
${}_5S_6$	-0.13	0.06	0.78	0.63	0.22	0.34	-0.15	-0.09	-0.51	-0.46	0.42	0.01	-0.74	-0.46	0.16	0.97	-0.23

Table 5e, degrees 2,4 cross-coupling interaction coefficient estimates

pair	c_2^0	re c_2^1	im c_2^1	re c_2^2	im c_2^2	c_4^0	re c_4^1	im c_4^1	re c_4^2	im c_4^2	re c_4^3	im c_4^3	re c_4^4	im c_4^4
${}_1S_3$-${}_3S_1$	0.39	-0.11	0.19	-0.81	-0.06	-0.06	-0.04	0.16	0.08	0.31	0.07	0.20	-0.14	0.07
${}_0S_{10}$-${}_0T_{11}$	1.07	0.78	-1.11	1.35	-1.47	.	.	.	.	.	.	.	.	.
${}_0S_{11}$-${}_0T_{12}$	1.73	1.66	1.33	1.82	0.52	.	.	.	.	.	.	.	.	.
${}_0S_{17}$-${}_0T_{18}$	2.57	1.51	-1.07	1.98	0.43	.	.	.	.	.	.	.	.	.
${}_0S_{19}$-${}_0T_{20}$	5.68	2.40	-2.83	2.65	1.44	-0.91	0.72	2.09	-0.93	-0.60	0.26	-1.20	0.41	-0.40
${}_0S_{20}$-${}_0T_{21}$	6.08	0.96	-1.08	3.12	-1.57	-0.51	0.27	1.50	1.26	-0.23	0.28	-1.08	0.40	1.86
${}_0S_{11}$-${}_2S_7$	.	.	.	.	.	-1.71	1.15	-1.35	0.49	-0.13	-1.91	-0.60	0.32	0.64

Table 5f, degree 6 cross-coupling interaction coefficient estimates

pair	c_6^0	re c_6^1	im c_6^1	re c_6^2	im c_6^2	re c_6^3	im c_6^3	re c_6^4	im c_6^4	re c_6^5	im c_6^5	re c_6^6	im c_6^6
${}_0T_{12}$-${}_2S_7$	-2.00	-0.06	-2.44	0.18	0.45	2.68	0.16	-1.48	1.06	0.40	3.03	-0.26	-0.33
${}_0S_{11}$-${}_2S_7$	-0.91	-0.91	0.06	0.09	1.94	-0.48	-0.93	-1.43	0.91	1.16	-0.60	1.11	0.52
${}_0S_{17}$-${}_2S_{11}$	-0.50	0.74	0.97	1.89	4.08	0.48	0.31	0.55	2.47	2.81	-1.67	1.28	-0.21
${}_0T_{20}$-${}_0S_{19}$	-1.51	0.75	0.43	1.39	-1.61	-0.34	-0.79	1.00	1.44	-0.70	-3.44	1.64	1.22

Table 5g, degrees 1,3 cross-coupling interaction coefficient estimates

pair	c_1^0	re c_1^1	im c_1^1	c_3^0	re c_3^1	im c_3^1	re c_3^2	im c_3^2	re c_3^3	im c_3^3
${}_1S_5$-${}_2S_4$	0.44	1.30	-0.40	-2.65	1.28	-0.73	0.02	-1.32	0.18	-0.69
${}_1S_6$-${}_2S_5$	0.45	1.70	-0.40	-3.05	0.88	-1.20	0.02	-1.82	0.39	-0.79
${}_6S_4$ ${}_2T_4$	0.36	0.07	-2.50	2.55	-0.46	-1.85	-1.65	0.19	-2.33	-1.68

Table 5h, degree 5 cross-coupling interaction coefficient estimates

pair	c_5^0	re c_5^1	im c_5^1	re c_5^2	im c_5^2	re c_5^3	im c_5^3	re c_5^4	im c_5^4	re c_5^5	im c_5^5
${}_1S_5$-${}_2S_4$	0.14	0.17	0.09	-0.28	0.53	-0.07	0.18	0.21	-0.50	0.38	0.11
${}_1S_6$-${}_2S_5$	0.11	-0.92	-0.02	-0.96	0.13	-0.37	-0.12	0.20	0.29	0.41	0.45
${}_2S_9$-${}_0S_{14}$	-1.80	1.49	-0.60	4.06	1.30	0.63	-0.99	-1.56	3.59	0.34	-0.19
${}_3S_8$-${}_6S_3$	1.26	1.78	-0.33	1.40	0.31	-1.26	-0.93	-1.62	0.46	1.04	0.08
${}_4S_4$-${}_1T_8$	-3.95	1.00	0.48	0.16	0.95	-1.15	0.63	-0.72	0.25	-0.18	-4.17
${}_5S_4$-${}_2T_4$	-3.61	0.19	0.47	0.64	1.46	0.96	1.65	-0.38	-0.64	1.92	-1.32

Table 5i, degree 7 cross-coupling interaction coefficient estimates

pair	c_7^0	re c_7^1	im c_7^1	re c_7^2	im c_7^2	re c_7^3	im c_7^3	re c_7^4	im c_7^4	re c_7^5	im c_7^5	re c_7^6	im c_7^6	re c_7^7	im c_7^7
${}_3S_8$-${}_6S_3$	0.74	-0.29	-0.49	0.39	0.40	0.33	-0.09	-0.19	-0.53	0.08	0.19	0.38	-0.59	-1.04	-1.36
${}_4S_4$-${}_1T_8$	-3.20	0.26	2.34	-0.36	-1.19	-0.30	-0.07	-1.17	2.00	0.30	0.56	0.17	1.96	-0.05	-0.43
${}_5S_4$ ${}_2T_4$	0.60	-0.80	-0.28	0.79	-0.15	0.15	-0.66	-0.18	1.25	-0.06	0.00	-0.72	0.06	-0.59	-0.11

Table 6: Effect on HSNR Misfits of degrees > 4 and coupling

target multiplets	HSNR MR		HSNR amp misfit (%)		HSNR phase misfit (°)	
	degrees 0-4	degrees 0-s_{max}	degrees 0-4	degrees 0-s_{max}	degrees 0-4	degrees 0-s_{max}
${}_0S_8$	.20	.13	5.0	4.5	4.1	3.5
${}_1S_8$	.19	.06	1.5	0.7	5.1	2.8
${}_2S_6$	.18	.12	11.8	7.9	3.7	2.0
${}_0S_{20}$-${}_0T_{21}$-${}_2S_{13}$	.37	.31	15.5	13.7	8.8	6.6
	only Coriolis coupling	all estimated coupling	only Coriolis coupling	all estimated coupling	only Coriolis coupling	all estimated coupling
${}_2S_5$-${}_1S_6$ (a)	.29	.10	15.0	2.5	7.6	2.5
${}_5S_4$-${}_2T_4$ (a)	.32	.13	8.8	4.7	8.8	3.1
${}_0T_{20}$-${}_0S_{19}$	.39	.31	15.8	13.8	9.5	7.9
${}_3S_8$-${}_6S_3$ (a)	.26	.10	10.1	6.1	9.9	5.6

Figure 1

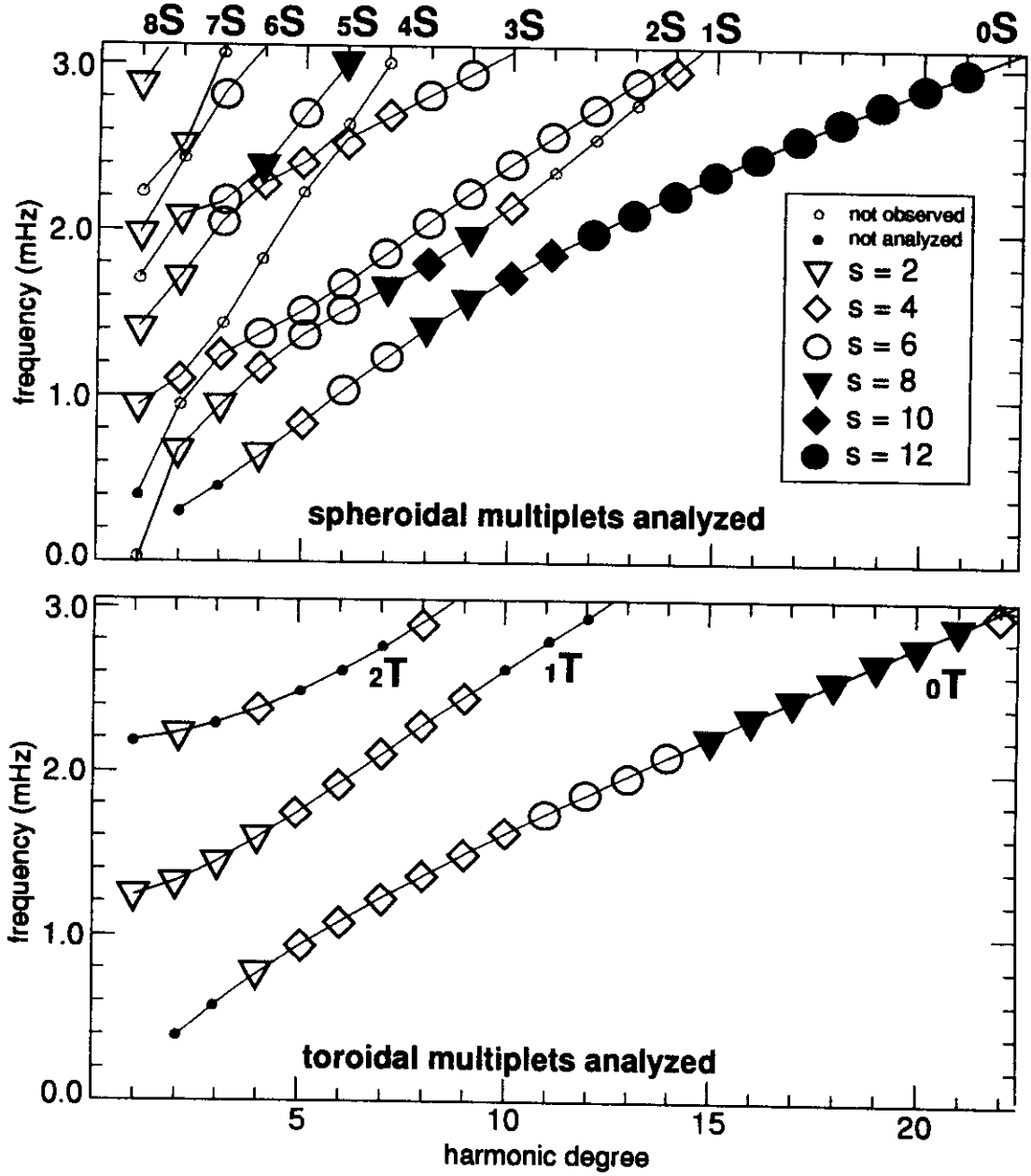
8S 7S 6S 5S 4S 3S 2S 1S 0S
3.0
2.0
1.0
0.0
frequency (mHz)
not observed
not analyzed
s = 2
s = 4
s = 6
s = 8
s = 10
s = 12
spheroidal multiplets analyzed
2T
1T
0T
toroidal multiplets analyzed
5
10
15
20
harmonic degree

Figure 2

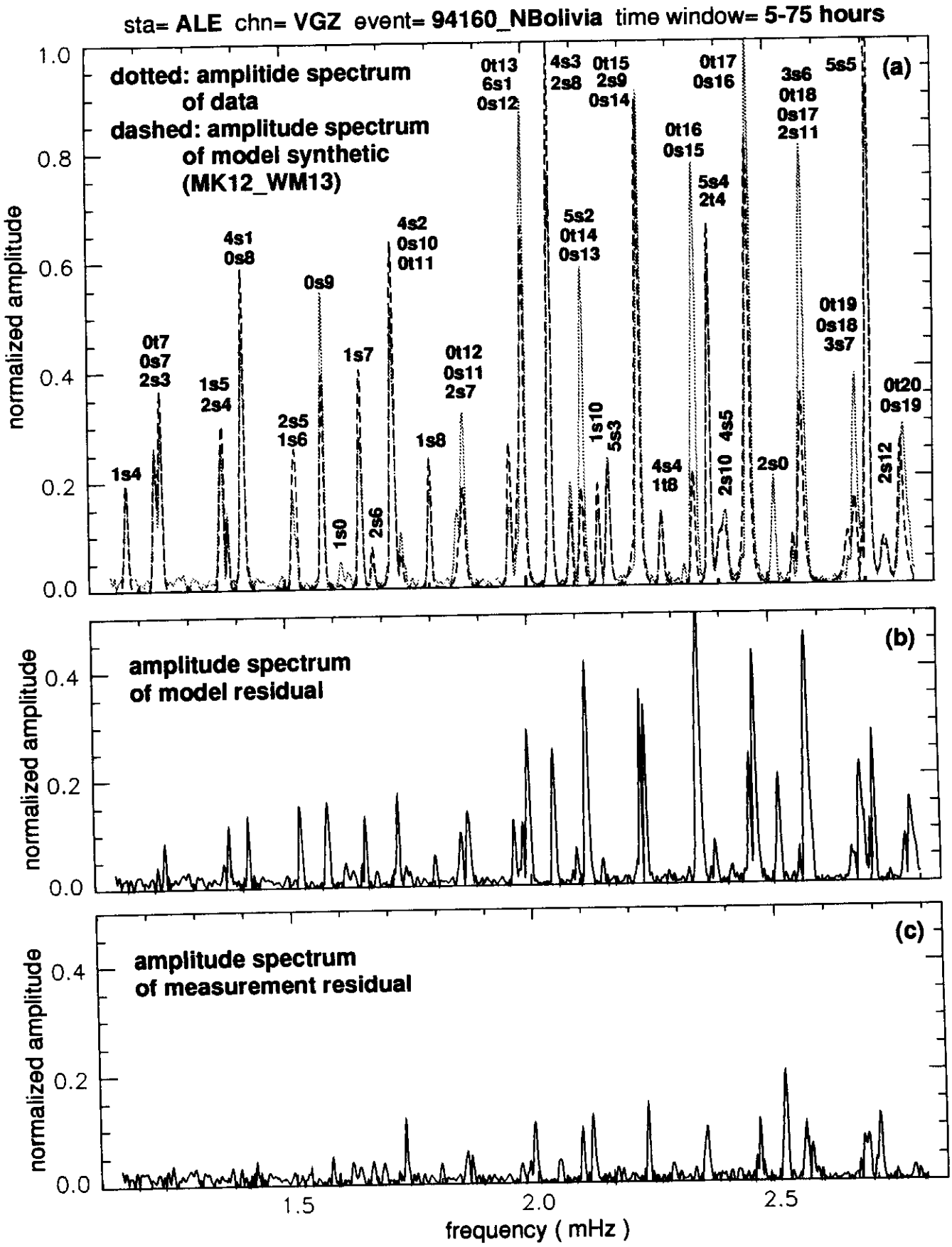
sta= ALE chn= VGZ event= 94160_NBolivia time window= 5-75 hours
dotted: amplitide spectrum of data
dashed: amplitude spectrum of model synthetic (MK12_WM13)
(a)
(b)
amplitude spectrum of model residual
(c)
amplitude spectrum of measurement residual
normalized amplitude
frequency (mHz)
1.0
0.8
0.6
0.4
0.2
0.0
1.5
2.0
2.5
1s4
0t7 0s7 2s3
1s5 2s4
4s1 0s8
2s5 1s6
0s9
1s0
1s7
2s6
4s2 0s10 0t11
1s8
0t12 0s11 2s7
0t13 6s1 0s12
4s3 2s8
5s2 0t14 0s13
0t15 2s9 0s14
1s10
5s3
4s4 1t8
0t16 0s15
0t17 0s16
5s4 2t4
4s5
2s10
2s0
3s6 0t18 0s17 2s11
5s5
0t19 0s18 3s7
2s12
0t20 0s19

Figure 3

correlation confidence comparisons of mantle v_S models

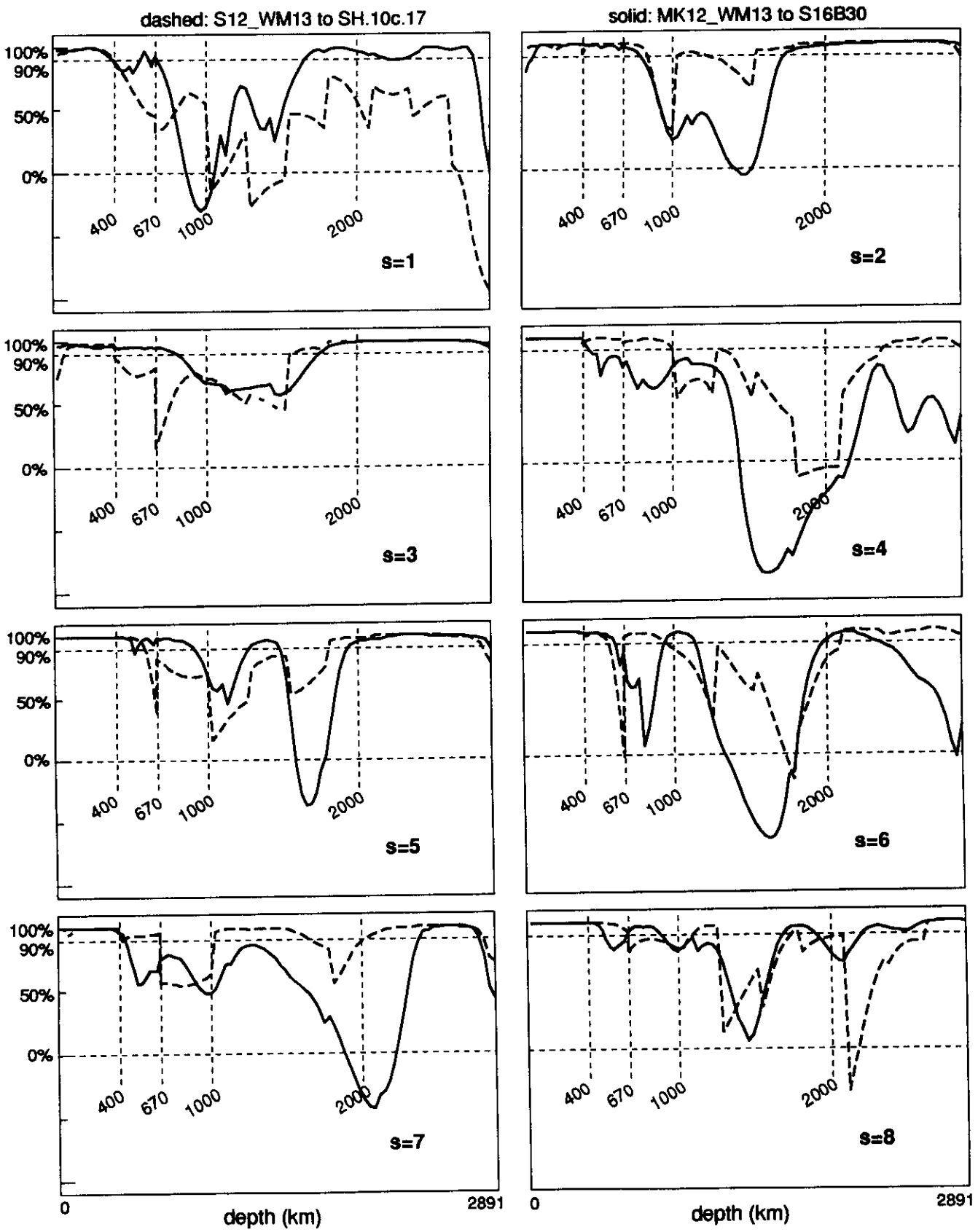

Figure 4

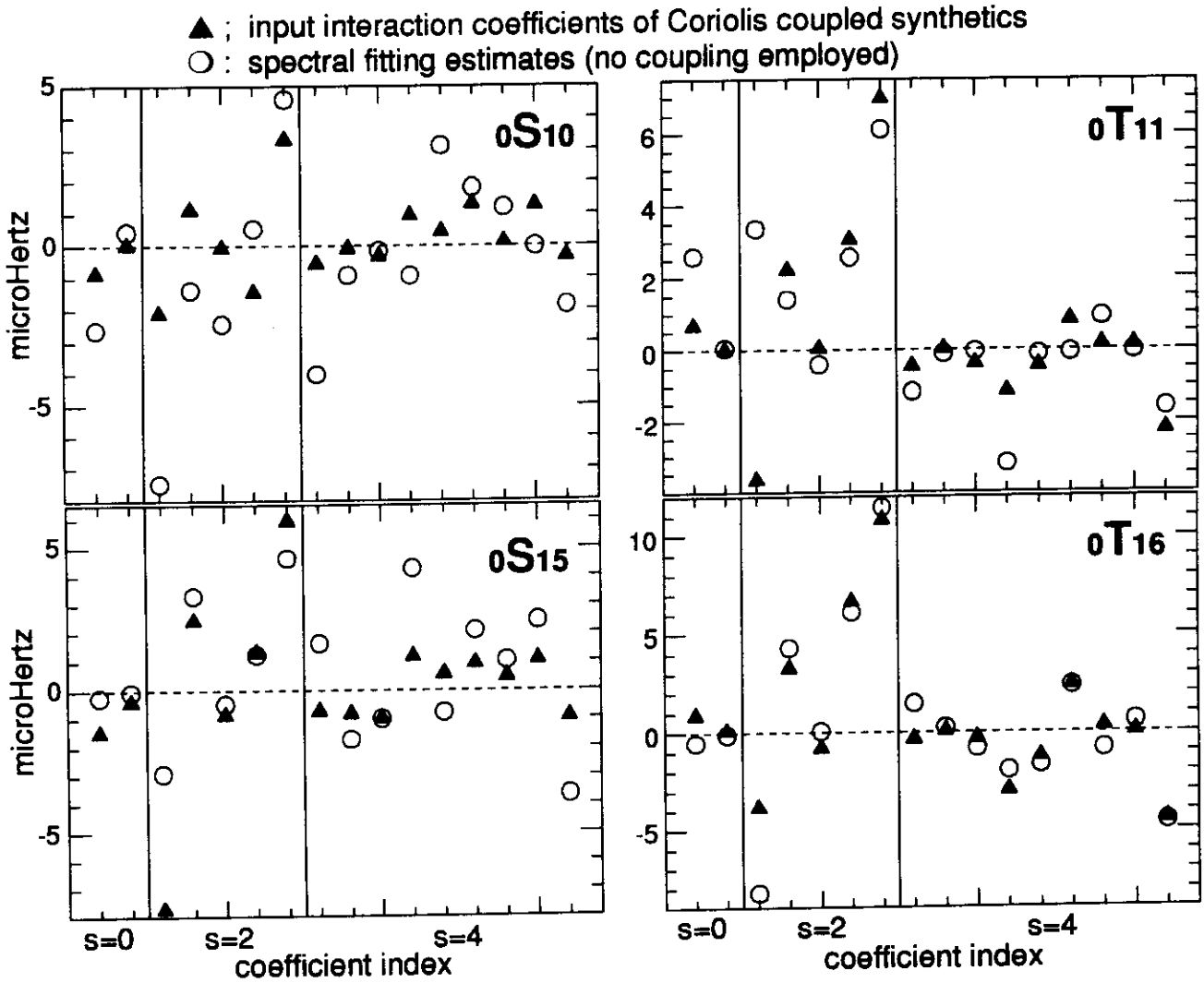
▲ ; input interaction coefficients of Coriolis coupled synthetics
○ : spectral fitting estimates (no coupling employed)
0S10
0S15
0T11
0T16
microHertz
microHertz
s=0
s=2
s=4
coefficient index
s=0
s=2
s=4
coefficient index

Figure 5

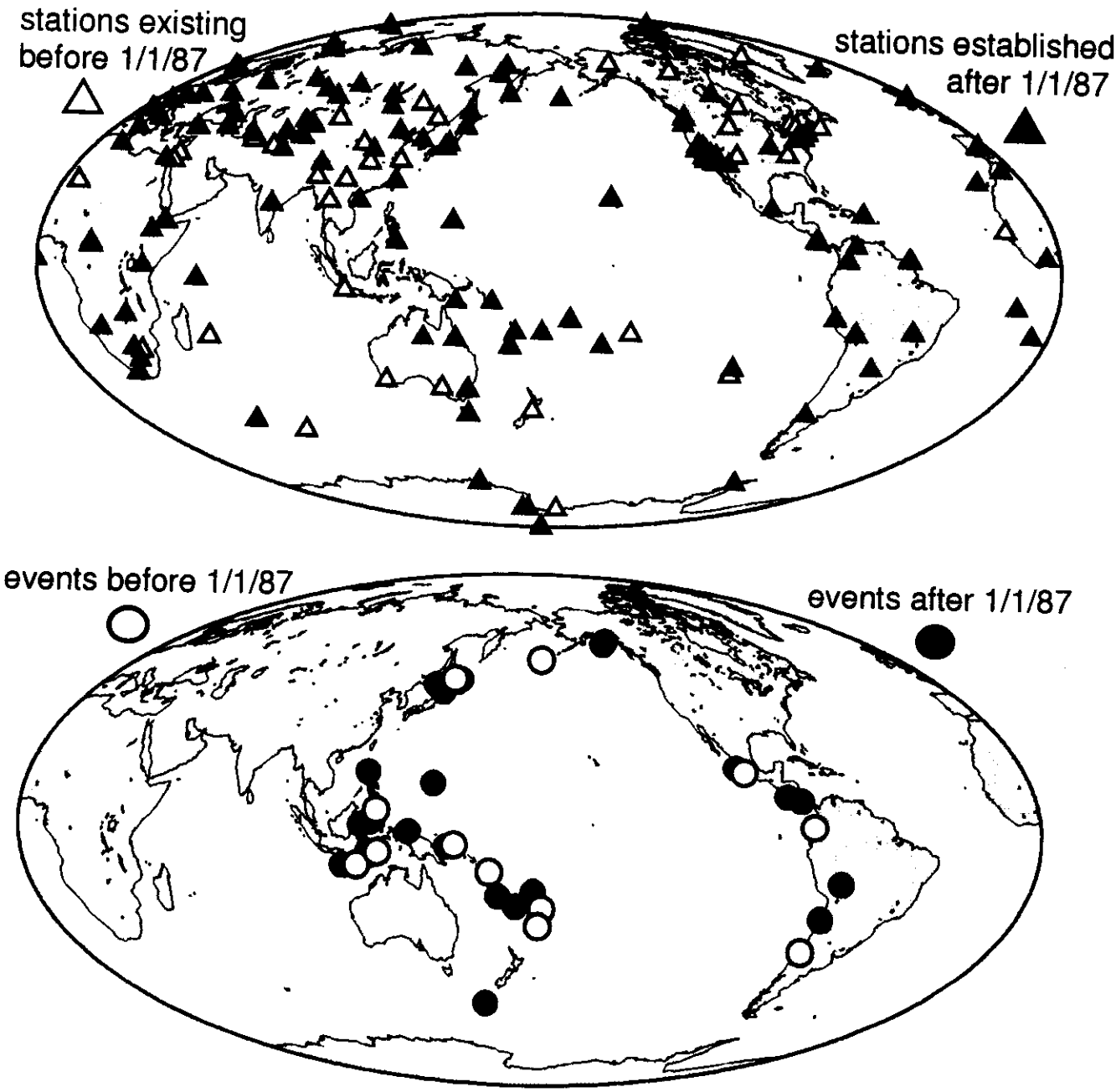
stations existing
before 1/1/87
stations established
after 1/1/87
events before 1/1/87
events after 1/1/87

Figure 6

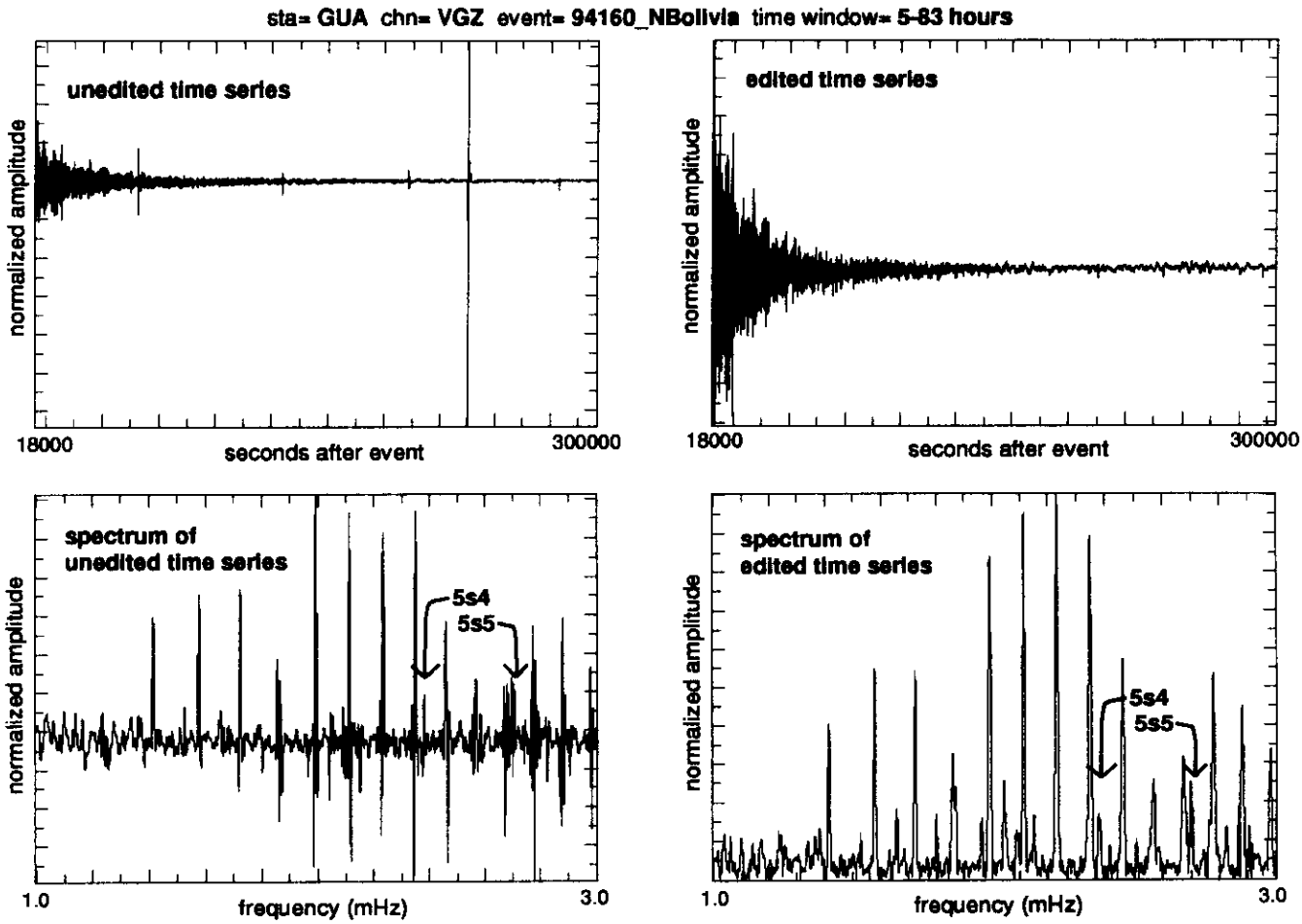
sta= GUA chn= VGZ event= 94160_NBolivia time window= 5-83 hours
unedited time series
normalized amplitude
18000
seconds after event
300000
edited time series
normalized amplitude
18000
seconds after event
300000
spectrum of
unedited time series
normalized amplitude
5s4
5s5
1.0
frequency (mHz)
3.0
spectrum of
edited time series
normalized amplitude
5s4
5s5
1.0
frequency (mHz)
3.0

Figure 7

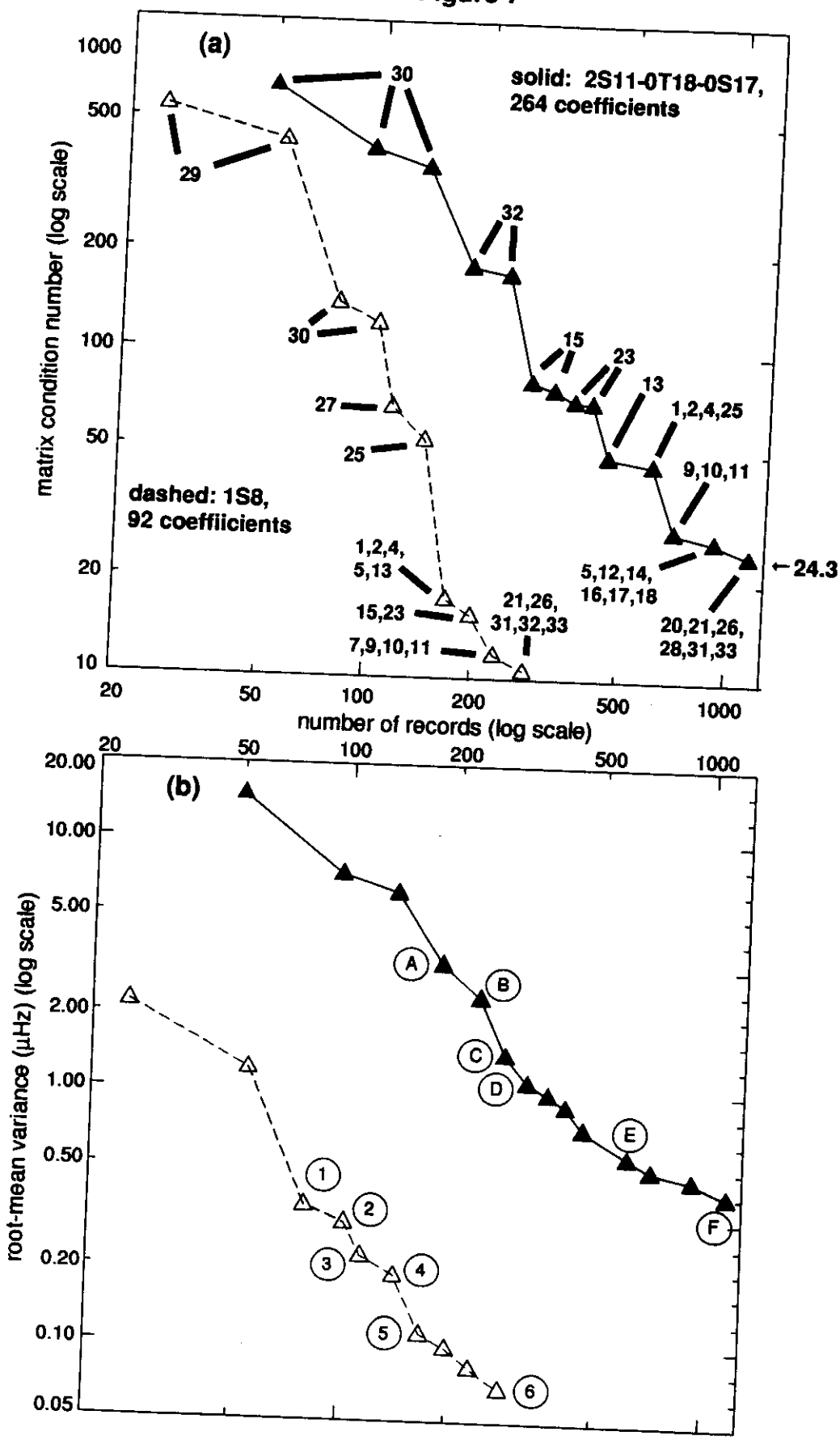
(a)
solid: 2S11-0T18-0S17,
264 coefficients
dashed: 1S8,
92 coefficients
matrix condition number (log scale)
number of records (log scale)
1000
500
200
100
50
20
10
20
50
100
200
500
1000
30
29
32
30
15
23
13
1,2,4,25
27
9,10,11
25
1,2,4,
5,13
5,12,14,
16,17,18
←24.3
15,23
21,26,
31,32,33
7,9,10,11
20,21,26,
28,31,33
(b)
root-mean variance (μHz) (log scale)
20.00
10.00
5.00
2.00
1.00
0.50
0.20
0.10
0.05
A
B
C
D
E
F
1
2
3
4
5
6

Figure 8

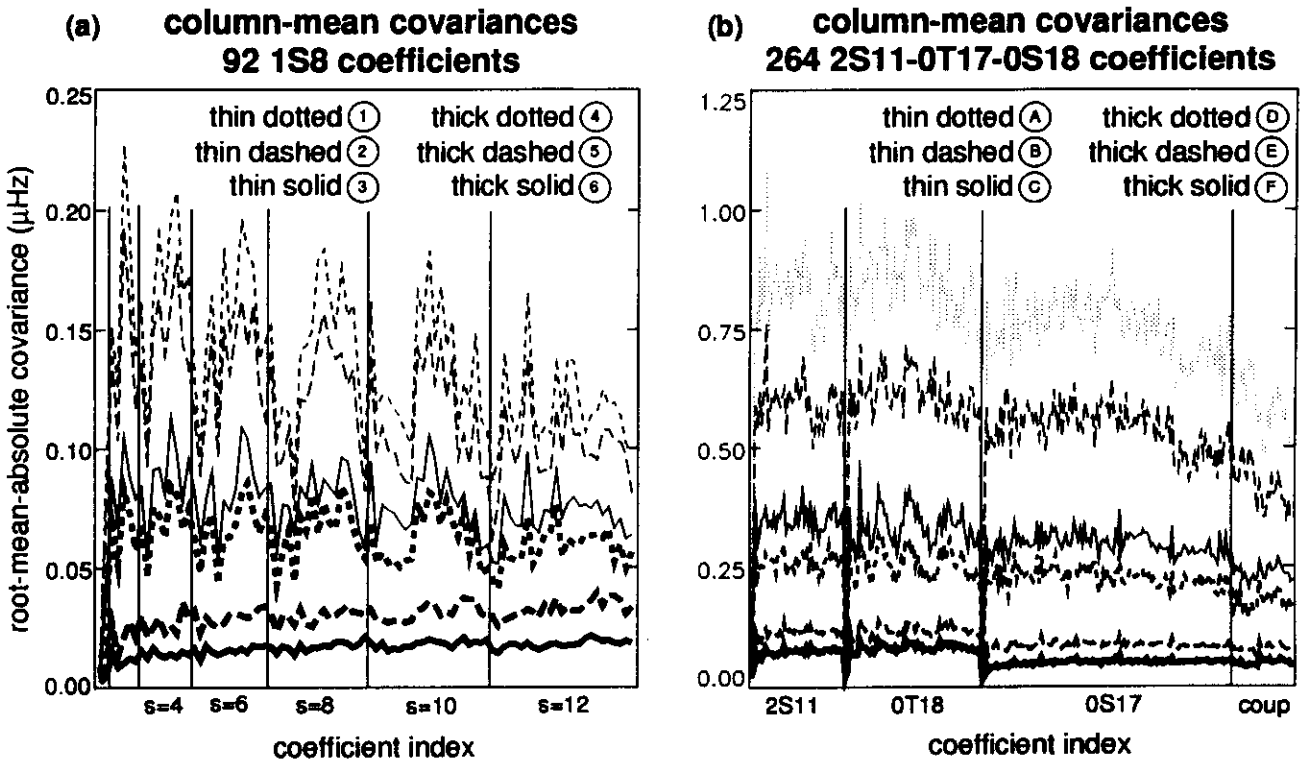
(a)
column-mean covariances
92 1S8 coefficients
thin dotted ①
thin dashed ②
thin solid ③
thick dotted ④
thick dashed ⑤
thick solid ⑥
root-mean-absolute covariance (μHz)
0.25
0.20
0.15
0.10
0.05
0.00
s=4
s=6
s=8
s=10
s=12
coefficient index
(b)
column-mean covariances
264 2S11-0T17-0S18 coefficients
thin dotted Ⓐ
thin dashed Ⓑ
thin solid Ⓒ
thick dotted Ⓓ
thick dashed Ⓔ
thick solid Ⓕ
1.25
1.00
0.75
0.50
0.25
0.00
2S11
0T18
0S17
coup
coefficient index

NORMALIZED COVARIANCE MATRICES

spectral fitting regressions for 92 1S8 interaction coefficients

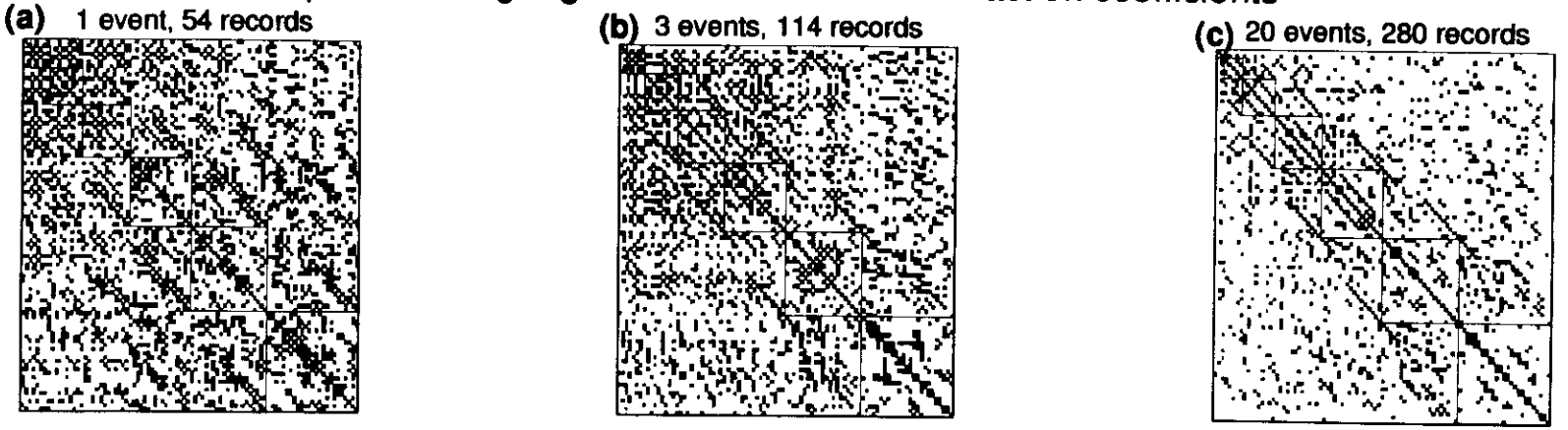

GSF regressions for 264 2S11-0T18-0S17 interaction coefficients

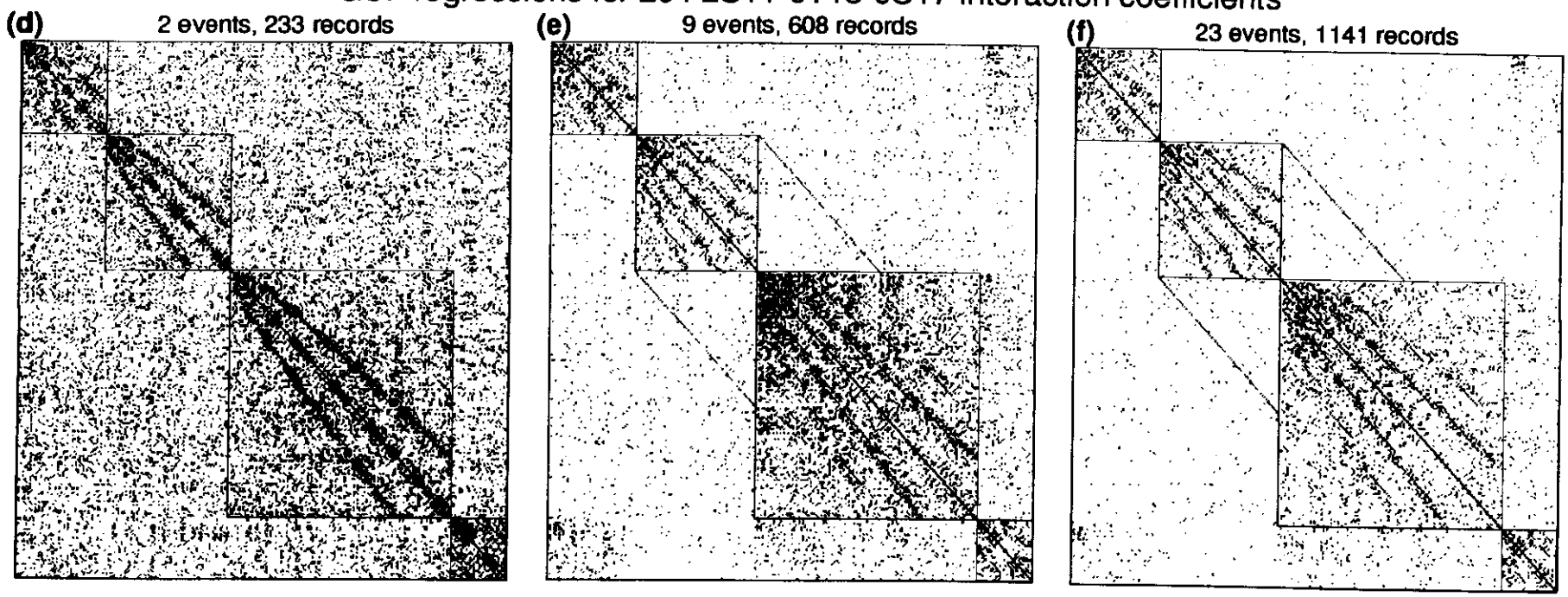

Figure 10

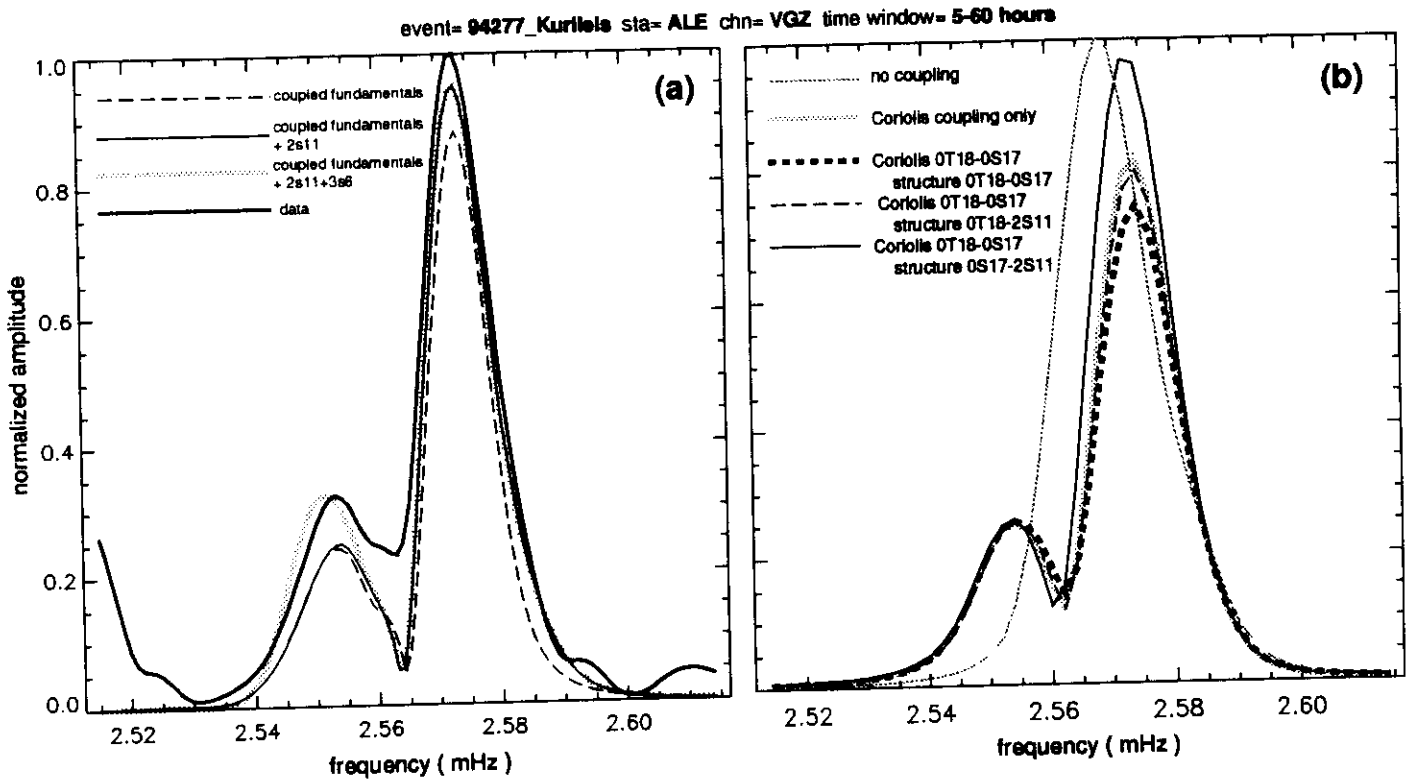
event= 94277_Kurilels sta= ALE chn= VGZ time window= 5-60 hours
(a)
coupled fundamentals
coupled fundamentals + 2s11
coupled fundamentals + 2s11+3s6
data
normalized amplitude
frequency (mHz)
(b)
no coupling
Coriolis coupling only
Coriolis 0T18-0S17 structure 0T18-0S17
Coriolis 0T18-0S17 structure 0T18-2S11
Coriolis 0T18-0S17 structure 0S17-2S11
frequency (mHz)

Figure 11

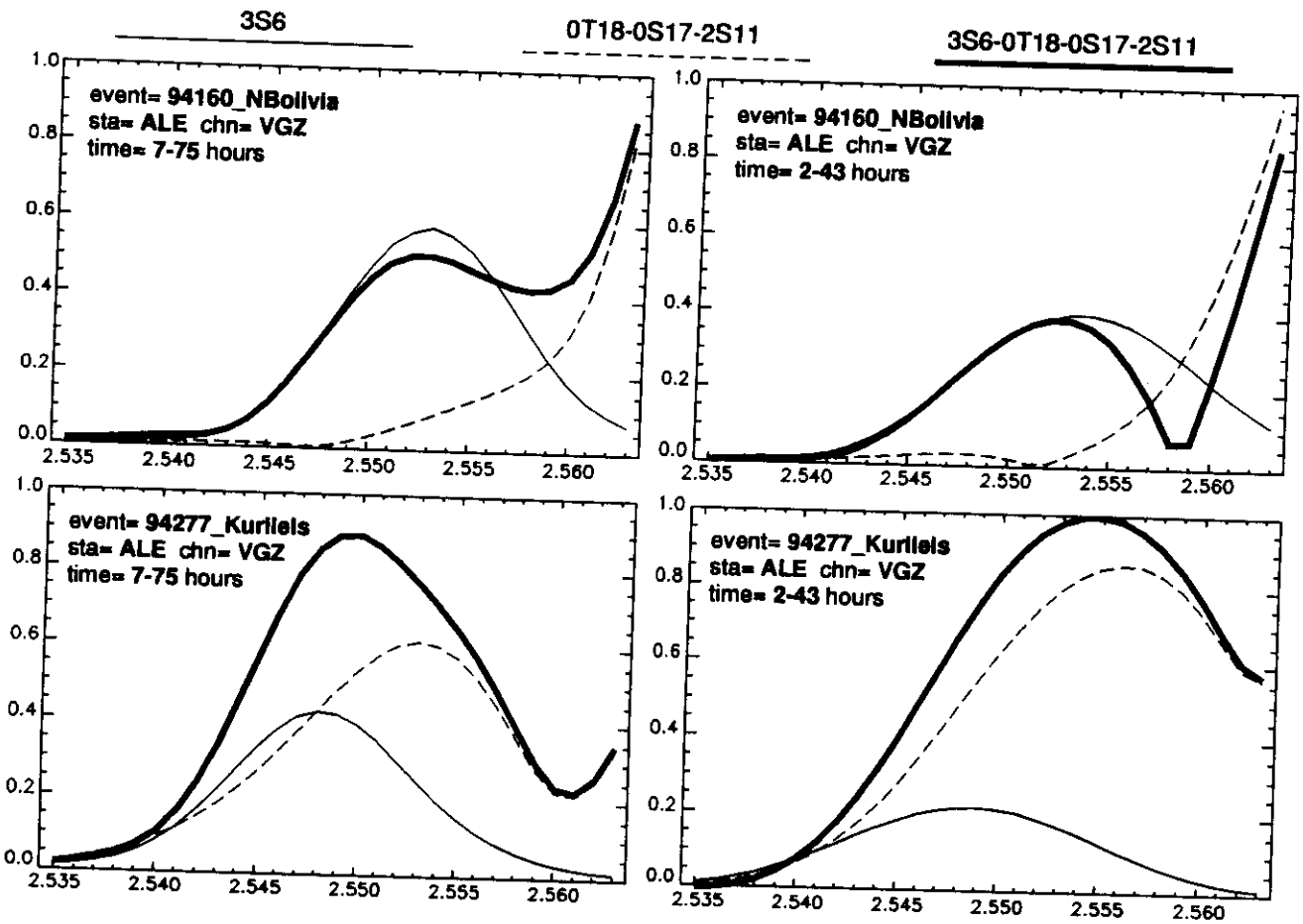
3S6
0T18-0S17-2S11
3S6-0T18-0S17-2S11
event= 94160_NBolivia
sta= ALE chn= VGZ
time= 7-75 hours
event= 94160_NBolivia
sta= ALE chn= VGZ
time= 2-43 hours
event= 94277_Kurilels
sta= ALE chn= VGZ
time= 7-75 hours
event= 94277_Kurilels
sta= ALE chn= VGZ
time= 2-43 hours
0.0
0.2
0.4
0.6
0.8
1.0
2.535
2.540
2.545
2.550
2.555
2.560

Figure 12: Plate A

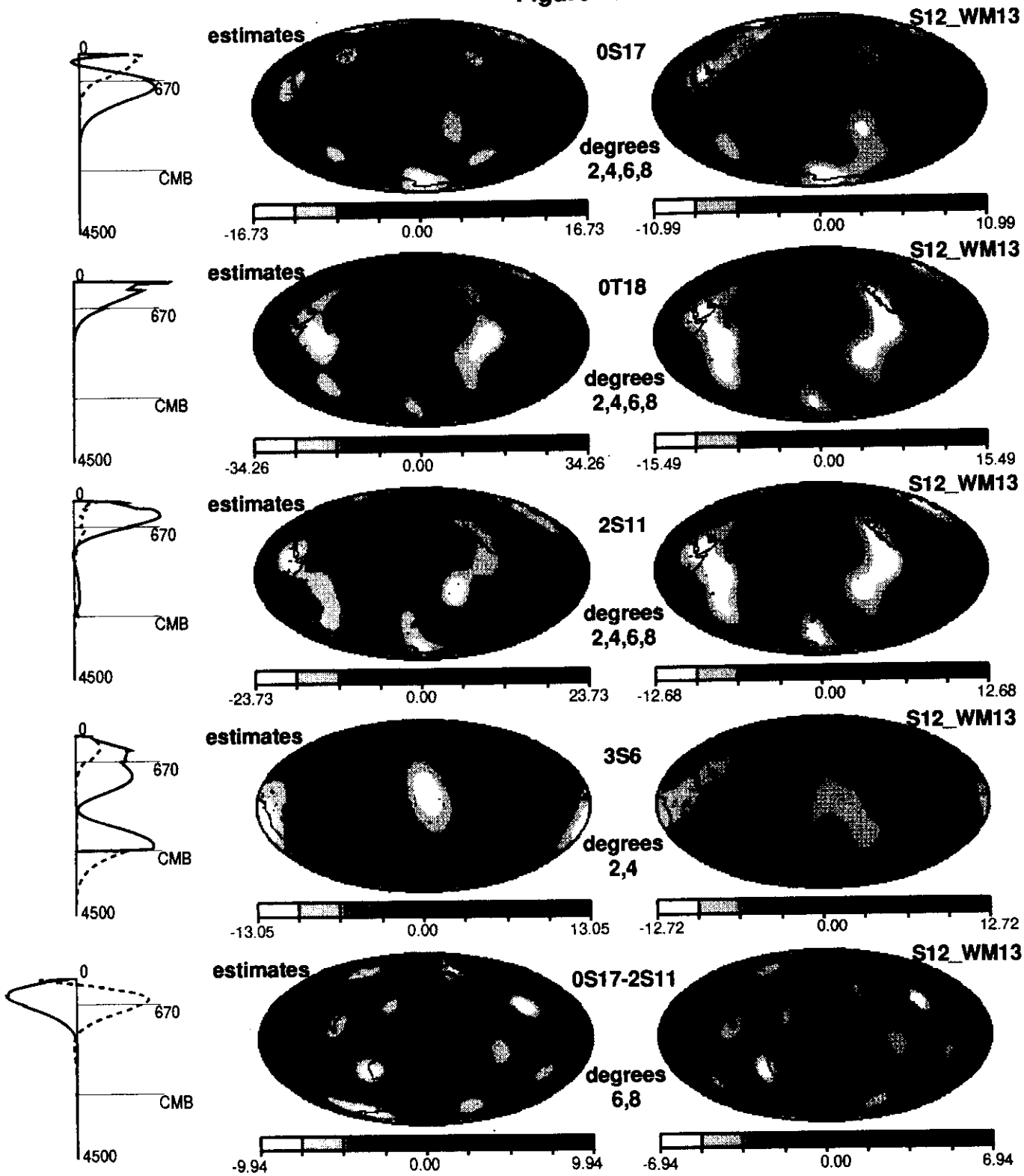

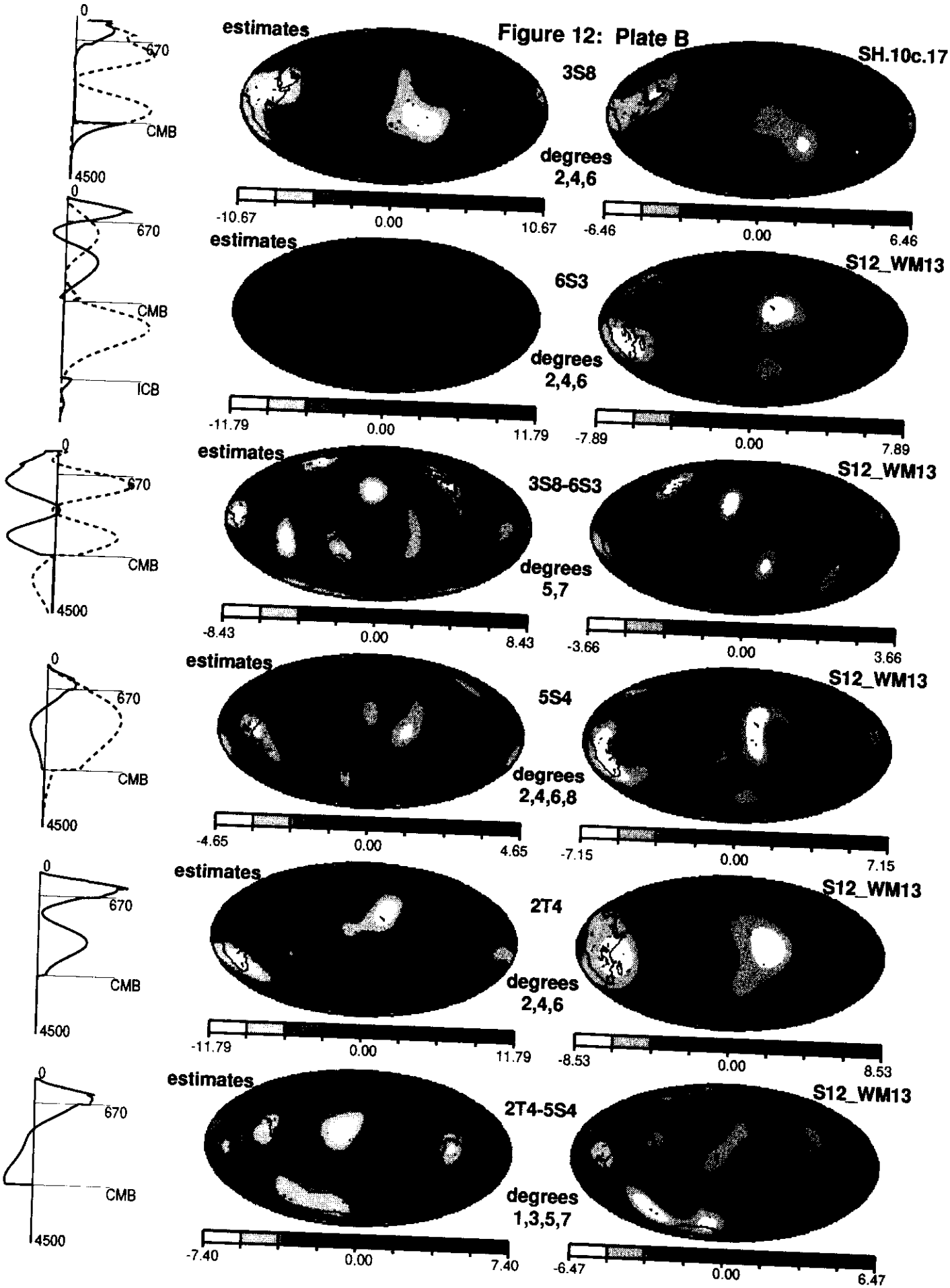
Figure 12: Plate B
estimates
3S8
SH.10c.17
degrees
2,4,6
-10.67
0.00
10.67
-6.46
0.00
6.46
estimates
6S3
S12_WM13
degrees
2,4,6
-11.79
0.00
11.79
-7.89
0.00
7.89
estimates
3S8-6S3
S12_WM13
degrees
5,7
-8.43
0.00
8.43
-3.66
0.00
3.66
estimates
5S4
S12_WM13
degrees
2,4,6,8
-4.65
0.00
4.65
-7.15
0.00
7.15
estimates
2T4
S12_WM13
degrees
2,4,6
-11.79
0.00
11.79
-8.53
0.00
8.53
estimates
2T4-5S4
S12_WM13
degrees
1,3,5,7
-7.40
0.00
7.40
-6.47
0.00
6.47
0
670
CMB
4500
0
670
CMB
ICB
0
670
CMB
4500
0
670
CMB
4500
0
670
CMB
4500
0
670
CMB
4500

Figure 12: Plate C

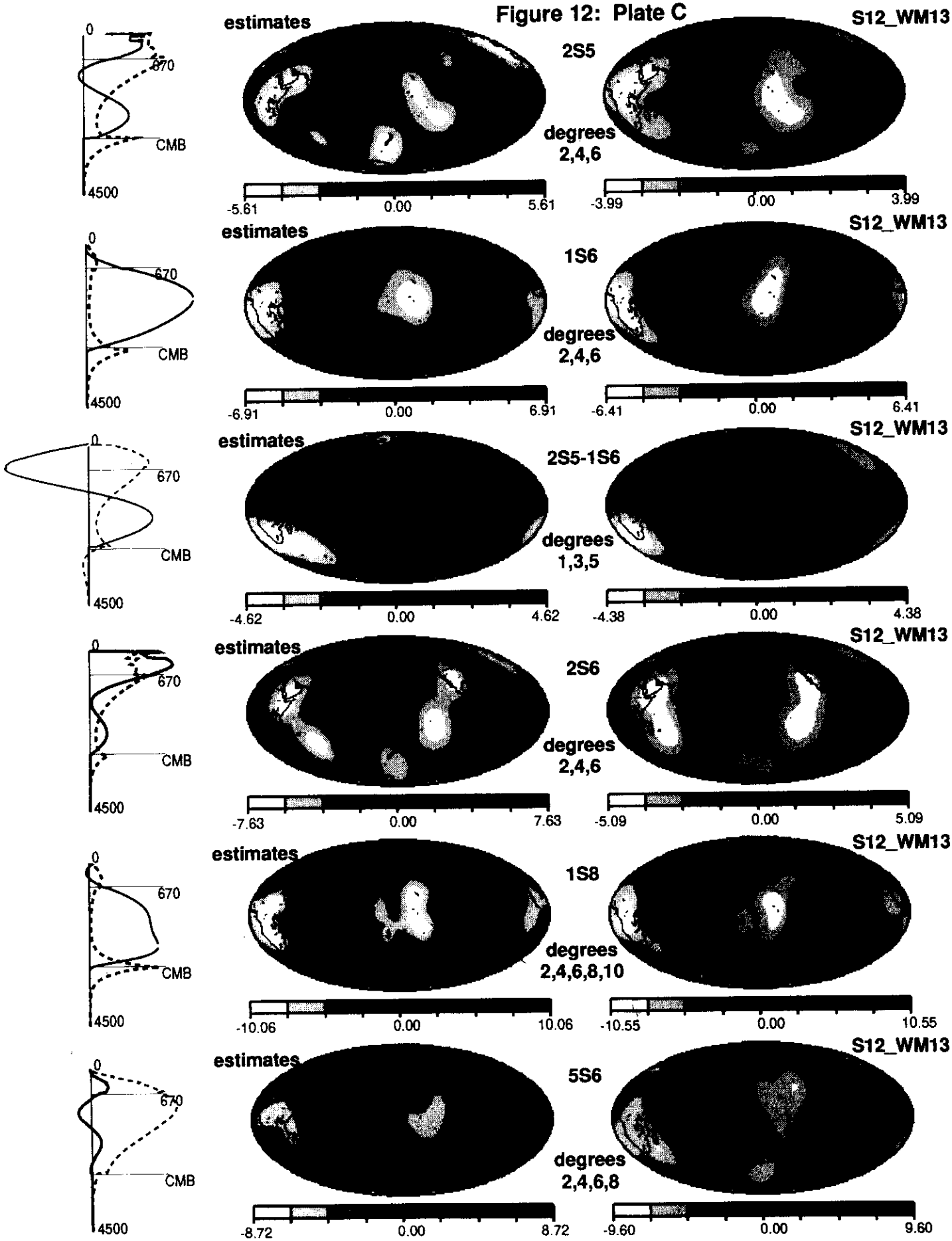

Figure 13

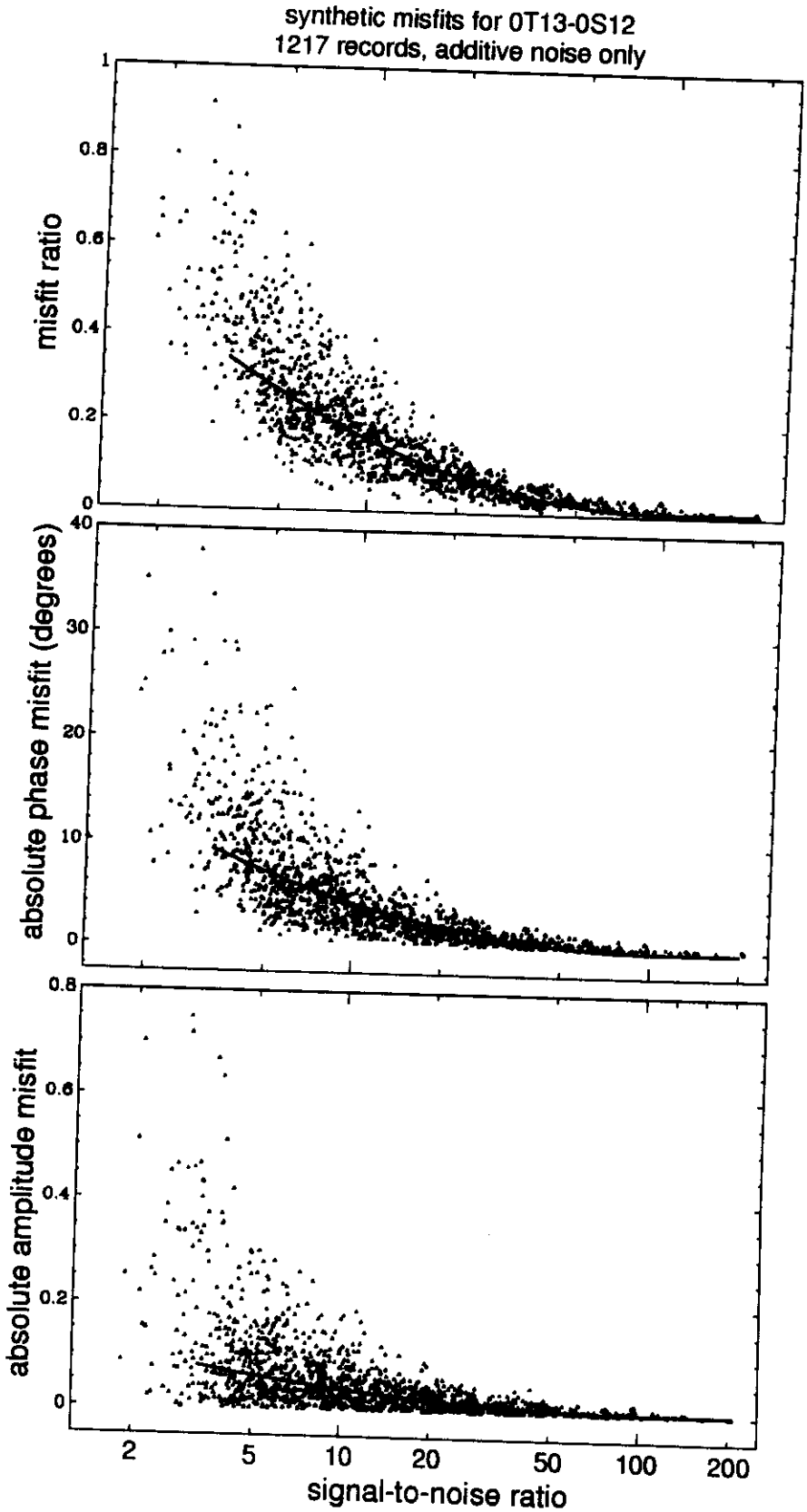
synthetic misfits for 0T13-0S12
1217 records, additive noise only
misfit ratio
absolute phase misfit (degrees)
absolute amplitude misfit
signal-to-noise ratio
2
5
10
20
50
100
200